IUCrJ
ISSN 2052-2525
CHEMISTRY | CRYSTENG

Semiconductive 2D arrays of pancake-bonded oligomers of partially charged TCNQ radicals

Krešimir Molčanov,[a]* Valentina Milašinović,[a] Biserka Kojić-Prodić,[a] Nadica Maltar-Strmečki,[a] Jiangyang You,[a] Ana Šantić,[b] Lidija Kanižaj,[c] Vladimir Stilinović[d] and Luka Fotović[d]

[a]Department of Physical Chemistry, Rudjer Bošković Institute, Bijenička 54, Zagreb 10000, Croatia, [b]Department of Materials Chemistry, Rudjer Bošković Institute, Bijenička 54, Zagreb 10000, Croatia, [c]Department of Materials Physics, Rudjer Bošković Institute, Bijenička 54, Zagreb 10000, Croatia, and [d]Department of Chemistry, Faculty of Science, University of Zagreb, Horvatovac 102a, Zagreb HR-10000, Croatia. *Correspondence e-mail: kmolcano@irb.hr

Received 14 September 2021
Accepted 3 May 2022

Edited by L. R. MacGillivray, University of Iowa, USA

Dedicated to the memory of Professor Stanko Popović, who passed away on 18 December 2020.

Keywords: multicentre two-electron bonding; TCNQ radical anions; pancake bonding; crystal structures; crystal engineering; magnetic properties; electrical properties.

CCDC references: 2105173; 2105174; 2105175; 2105176; 2105178; 2105179; 2105180; 2105181; 2105182; 2105183; 2105184; 2105185; 2105186; 2105187; 2105188; 2105189; 2105190; 2105191; 2105186

Supporting information: this article has supporting information at www.iucrj.org

Multicentre two-electron (mc/2e or 'pancake bonding') bonding between 7,7,8,8-tetracyanoquinodimethane (TCNQ) radical anions was studied on its 14 novel salts with planar organic cations. The formal charges of the $TCNQ^{\delta-}$ moieties are −1/2 and −2/3, and they form mc/2e bonded dimers, trimers and tetramers which are further stacked into extended arrays. Multicentre bonding within these oligomers is characterized by short interplanar separations of 2.9–3.2 Å; distances between the oligomers are larger, typically >3.3 Å. The stacks are laterally connected by C—H···N hydrogen bonding, forming 2D arrays. The nature of mc/2e bonding is characterized by structural, magnetic and electrical data. The compounds are found to be semiconductors, and high conductivity [10^{-2} $(\Omega\ cm)^{-1}$] correlates with short interplanar distances between pancake-bonded oligomers.

1. Introduction

π-Stacking of planar organic radicals is known to involve spin pairing of contiguous radicals (Preuss, 2014; Kertesz, 2019; Molčanov & Kojić-Prodić, 2019; Molčanov *et al.*, 2019*c*), as shown by the diamagnetic or antiferromagnetic properties of bulk samples (Molčanov & Kojić-Prodić, 2019; Molčanov *et al.*, 2019*c*). This implies the formation of a weak covalent interaction (Huang & Kertesz, 2007; Huang *et al.*, 2008; Novoa *et al.*, 2009; Tian & Kertesz, 2011; Preuss, 2014; Cui *et al.*, 2014*a*,*b*,*c*; Mou & Kertesz, 2017; Kertesz, 2019; Molčanov & Kojić-Prodić, 2019; Molčanov *et al.*, 2019*c*) with a non-localized electron pair distributed between two rings (Kertesz, 2019; Molčanov & Kojić-Prodić, 2019). Commonly used terms for this type of interaction are two-electron multicentre (mc/2e) bonding and pancake bonding (Preuss, 2014; Kertesz, 2019). According to quantum chemical models, an HOMO spanning both rings is formed (Kertesz, 2019) and the covalent contribution to the total interaction may exceed −15 kcal mol^{-1}, which is comparable to strong hydrogen bonding (Steiner, 2002; Kojić-Prodić & Molčanov, 2008). Therefore, pancake bonding may be regarded as both a strong intermolecular interaction and a weak covalent bond. It is interesting from both fundamental (the nature of chemical bonding) and practical (design of organic magnets and conductive materials) aspects (Podzorov, 2010; Hicks, 2011; Sanvito, 2011*a*,*b*; Veciana, 2011; Ratera & Veciana, 2011; Morita *et al.*, 2013; Murata *et al.*, 2013).

The most important factors for designing functional materials are stability and a low HOMO–LUMO energy barrier, which limits conductivity. It is known that electrons can easily

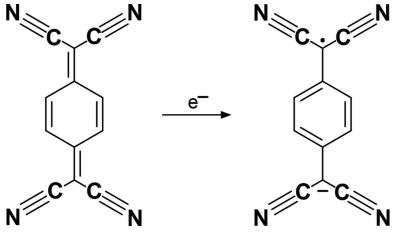

jump between two rings in a pancake-bonded dimer, whereas non-bonding stacking contacts (between the dimers) prevent electron jumping due to high energy barriers (Molčanov *et al.*, 2019*a*). Thus, conductivity can be enhanced if pancake bonding is extended throughout a crystal. We have shown that, in infinite stacks of equidistant radicals, pancake bonding extends not only between a pair of radicals, but throughout a stack (Molčanov *et al.*, 2019*a*,*c*; Molčanov & Kojić-Prodić, 2019), and such crystals are semiconductive (Molčanov *et al.*, 2016; 2018*a*). For ionic radical systems, conductivity rarely exceeds 10^{-6} S cm^{-1} (Itkis *et al.*, 2002; Lekin *et al.*, 2010; Podzorov, 2010; Mercuri *et al.*, 2010; Sanvito, 2011*b*; Yu *et al.*, 2011, 2012; Morita *et al.*, 2013; Murata *et al.*, 2013; Nakano, 2014; Chen *et al.*, 2016; Molčanov *et al.*, 2016; 2018*a*), but neutral radicals tend to be better conductors, with conductivity reaching 10^{-1} S cm^{-1} (Itkis *et al.*, 2002; Podzorov, 2010; Mercuri *et al.*, 2010; Lekin *et al.*, 2010; Sanvito, 2011*b*; Yu *et al.*, 2011, 2012; Morita *et al.*, 2013; Murata *et al.*, 2013; Nakano, 2014; Alemany *et al.*, 2015; Chen *et al.*, 2016).

The stability of a solid-state radical system depends mostly on the stability of the radical. Therefore, planar radicals with extensive delocalization of π-electrons are most widely used in crystal engineering, for example, derivatives of tetrathia- and tetraselenafulvalene (Ganesan *et al.*, 2003; Bendikov *et al.*, 2004; Rosokha & Kochi, 2007; Mercuri *et al.*, 2010; Morita *et al.*, 2013; Murata *et al.*, 2013), and semiquinones (Rosokha & Kochi, 2007; Rosokha *et al.*, 2009; Molčanov *et al.*, 2016; 2018*a*, 2019*b*).

One of the most stable and extensively studied organic radicals is 7,7,8,8-tetracyanoquinodimethane (TCNQ, neutral and radical forms are shown below), a strong electron

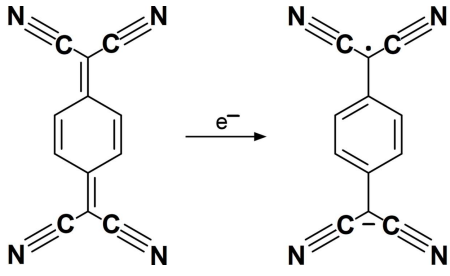

acceptor suitable for the formation of salts. It comprises a six-membered ring similar to the quinones (Hünig, 1990) and is stabilized by four electron-withdrawing cyano groups. It also readily forms pancake bonds. However, unlike the semiquinones, which usually form negatively charged radicals with a total charge of −1 (Molčanov *et al.*, 2012, 2016, 2018*a*, 2019*a*,*c*; Molčanov & Kojić-Prodić, 2019), TCNQ is, in its salts, often only partially charged (its formal charge being −1/2 or −2/3), implying a partial radical character of the TCNQ$^{\delta-}$ moiety. Increasing negative charge enhances the delocalization of the π electrons; formally double bonds (*a* and *c* in Fig. 1) are elongated, whereas formally single bonds (*b* and *d* in Fig. 1) are shortened compared with the neutral compound. To estimate the charge of the TCNQ$^{\delta-}$ moiety, correlations of these bond lengths have been proposed, for example $c/(b+d)$

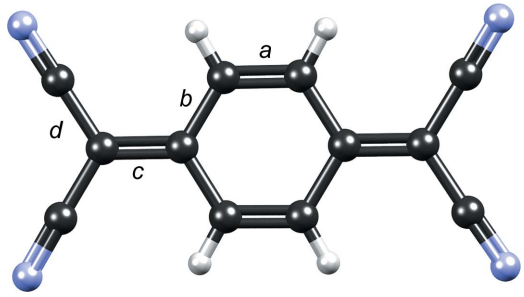

Figure 1
Lettering denotes the different types of C—C bonds in the TCNQ$^{\delta-}$ radical used for geometric correlation between the bond lengths and charge of the ring. With increasing negative charge and radical character, bonds *a* and *c* are elongated, whereas bonds *b* and *d* are shortened.

(Kistenmacher *et al.*, 1982). In a review of a larger number of compounds containing TCNQ, Herbstein & Kapon (2008) used differences in bond lengths *b*–*a* and *c*–*d*. Their respective values for the neutral compound are 0.096 and −0.052 Å and for a negatively charged (−1) anion radical are 0.068 and −0.012 Å. However, owing to a variety of reasons, these are of limited reliability (see the Results and discussion).

To date, over 1000 crystal structures containing TCNQ in various oxidation states, ranging from 0 to −1, have been published (Groom *et al.*, 2016). A detailed review was published by Harms *et al.*(1982). Thus, a systematic analysis of crystal packing and molecular interactions is beyond the scope of this paper; here we discuss only structures with π-interactions between the TCNQ moieties, but not mixed stacks involving electron donors and acceptors, represented by a well known molecular complex of TCNQ with tetrathiafulvalene (TTF) (Schultz *et al.*, 1976).

Unlike semiquinones, which usually form stacks of pancake-bonded dimers (or, more rarely, stacks of equidistant radicals) (Molčanov *et al.*, 2018*a*; 2019*a*,*b*; Molčanov & Kojić-Prodić, 2019), TCNQ$^{\delta-}$ radicals form different types of pancake-bonded oligomers and a wide variety of long-range ordering. In many structures, isolated pancake-bonded dimers (which form no stacking interaction with neighbouring molecules) are present (Keller *et al.*, 1981; Harms *et al.*, 1982; Abashev *et al.*, 1987; Miller *et al.*, 1987; O'Hare *et al.*, 1990; Stein *et al.*, 1991; Grossel & Weston, 1992; Chen *et al.*, 2008; Sutton *et al.*, 2016; Park *et al.*, 2018). Sometimes the dimers form 1D stacks similar to those of semiquinones (Hoekstra *et al.*, 1972; Ashwell *et al.*, 1975*a*, 1977*a*; Bosch & Bodegom, 1977; Endres *et al.*, 1978,*b*; Diezt *et al.*, 1981; Konno & Saito, 1981; Waclawek *et al.*, 1983; Visser *et al.*, 1990*a*,*b*,*c*,*d*,*e*; Magonov *et al.*, 1991; Ballester *et al.*, 1997; Moore *et al.*, 2001; Mukai *et al.*, 2001; Nishimura *et al.*, 2002; Chen *et al.*, 2008; Qu *et al.*, 2011; Martin *et al.*, 2012; Lu *et al.*, 2017; Üngör *et al.*, 2021*a*), but also planar 2D arrays have been described (Ashwell *et al.*, 1982, 1983; Bryce *et al.*, 1988; Brook & Koch, 1997; Radváková *et al.*, 2010; Qu *et al.*, 2011); in some of these structures the formal charge (*i.e.* charge derived from stoichiometry) of TCNQ is −1/2 (Ashwell *et al.*, 1977*a*, 1982). Pancake-bonded trimers, which often form stacks, are quite common, with a formal charge on the TCNQ$^{\delta-}$ moiety of −2/3 (Ashwell *et al.*, 1977*b*; Endres *et al.*, 1978*a*,*b*; Ashwell & Wallwork, 1979; Sandman *et*

al., 1980; Lau *et al.*, 1982; Bell *et al.*, 1991; Usov *et al.*, 1991; Akutagawa *et al.*, 1996, 2004; Bigoli *et al.*, 1996; Ballester *et al.*, 2000; Nishijo *et al.*, 2004; Chen *et al.*, 2007; Liu *et al.*, 2008; Mochida *et al.*, 2008; Martin *et al.*, 2012; Kubota *et al.*, 2014; Phan *et al.*, 2015). However, different bond lengths in the central and lateral rings of a trimer indicate different total charge of the rings, which can be estimated using geometric correlations (see above). For example, in the compound $(MT)_2(TCNQ)_3{\cdot}2H_2O$ (MT = *S*-methilthiouronium) the charges on the central ring and the lateral rings were estimated to be −0.9 and −0.4, respectively; the total charge of a trimer is thus −1.7 (Usov *et al.*, 1991). In a 2:3 salt of *N*,*N*-dimethyl-D-proline-methylester and $TCNQ^{\delta-}$ the rings form a trimer stack in the sequence ...*ABB*... with the charge of *A* being −0.30 and of *B* being −0.94 [thus, the charge of the trimer is −2.18 (Martin *et al.*, 2012)]. The trimers are usually centrosymmetric, and the central ring is usually more negatively charged than the lateral rings. In our previous studies we noted a similar distribution of charge in trimers of semiquinone radicals (Molčanov *et al.*, 2018*b*; 2019*b*).

There are also tetramers, usually composed of $TCNQ^{\delta-}$ moieties with a formal charge of −1/2 [therefore, a tetramer has a charge of −2, implying paired spins (Ashwell & Nowell, 1984; Ashwell & Wallwork, 1985; Rindorf *et al.*, 1988; Takagi *et al.*, 1994; Malatesta *et al.*, 1995)]. These tetramers can stack, forming 1D (Ashwell *et al.*, 1977*c*,*d*; Filhol *et al.*, 1980; Filhol & Thomas, 1984; Üngör *et al.*, 2021*b*) or 2D arrays (Kubota *et al.*, 2014). Stacks of equidistant radicals, which involve long-range antiferromagnetic ordering and semiconductive properties have also been described for a number of compounds (Shirotani & Kobayashi, 1973; Kistenmacher *et al.*, 1974; van Bodegom *et al.*, 1977; Endres, 1982; Bryce *et al.*, 1990; Visser *et al.*, 1990*f*; Murata *et al.*, 2007; Chen *et al.*, 2008; Liu *et al.*, 2011). Less common are stacked pentamers (Ashwell *et al.*, 1977*c*,*d*, 1978; Lu *et al.*, 2011) and structures comprising two different types of stacks (Ashwell *et al.*, 1978; Murata *et al.*, 2006).

Studying the nature of multicentre covalent bonding between $TCNQ^{\delta-}$ radicals requires correlation of the crystal structures with magnetic and electric properties. Analogous to the detailed studies of stacked semiquinones, it can be established with certainty that structures of pancake-bonded dimers and trimers with a total charge of −2 are diamagnetic and insulators, and that those of equidistant radicals are semiconductors with long-range magnetic order [most likely antiferromagnetic (Molčanov *et al.*, 2012, 2016, 2018*a*,*b*, 2019*c*; Molčanov & Kojić-Prodić, 2019]. However, little can be said of the magnetic and electric properties of 2D arrays of dimers $(TCNQ)_2^-$ with a total charge of −1 (these contain a single unpaired electron) and tetramers of radicals, which do not have a well studied quinoid analogue. To determine properties of multicentre bonding in such systems, we prepared and characterized a series of fourteen novel salts of the $TCNQ^{\delta-}$ radical anion with planar organic cations.

2. Results and discussion

A series of salts of the partially charged $TCNQ^{\delta-}$ radical anion with the following organic cations was prepared: 2-bromo-*N*-methylpyridinium (**1**), 2-methyl-*N*-methylpyridinium (**2**), 3-iodo-*N*-methylpyridinium (**3**), 4-benzoyl-*N*-methylpyridinium (**4**), 4-dimethylamino-*N*-methylpyridinium (**5**), 4-iodo-*N*-methylpyridinium (**6**), 4-methyl-*N*-methylpyridinium (**7**), 3,5-dibromo-*N*-ethylpyridinium (**8**), *N*,*N*′-diethyl-4,4′-bipyridinium (**9**), *N*,*N*′-dimethyl-4,4′-bipyridinium (**10**), 3-bromo-*N*-methylpyridinium (**11**), 3,5-dibromo-*N*-methylpyridinium (**12**), *N*-methylpyridinium (**13**) and *N*-methyl-1,10-phenanthrolinium (**14**) (see below).

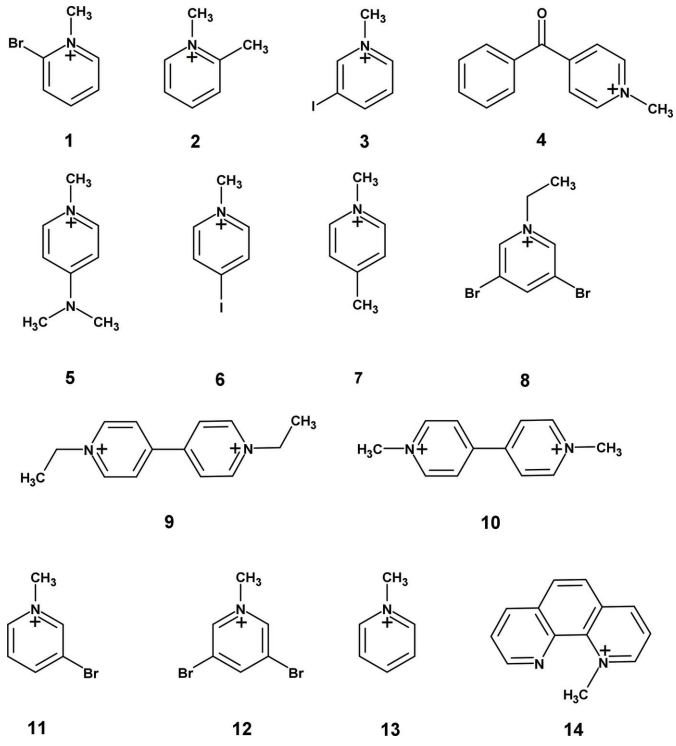

In the majority of the compounds there are two $TCNQ^{\delta-}$ moieties per one cation (or four in the case of the divalent *N*,*N*′-diethyl-4,4′-bipyridinium cation), so the stoichiometries are **2**·$(TCNQ)_2$, **3**·$(TCNQ)_2$, **4**·$(TCNQ)_2$, **5**·$(TCNQ)_2$, **6**·$(TCNQ)_2$, **7**·$(TCNQ)_2$, **8**·$(TCNQ)_2$, **9**·$(TCNQ)_4$, **12**·$(TCNQ)_2$, **13**·$(TCNQ)_2$ and **14**·$(TCNQ)_2$. Two compounds include halide anions: $\mathbf{1}_2{\cdot}Br{\cdot}(TCNQ)_2$ and $\mathbf{11}_2{\cdot}I{\cdot}(TCNQ)_2$, and one crystallized with a stoichiometry of 1:3, **10**·$(TCNQ)_3$.

2.1. Structure and charge of the $TCNQ^{\delta-}$ radical

Stoichiometries of the studied compounds indicate that the charge of $TCNQ^{\delta-}$ is −1/2, except in **10**·$(TCNQ)_3$ where it is −2/3. Molecular geometry (Table S1 of the supporting information) and IR spectra (Table 1) are in agreement with the partial charge and partial radical character of the $TCNQ^{\delta-}$ moieties. It is known that with increasing negative charge and radical character, the molecular structure of $TCNQ^{\delta-}$ and related quinones change from quinoid towards semiquinoid: formally double bonds (*a* and *c* in Fig. 1) are elongated whereas formally single bonds (*b* and *d* in Fig. 1) are shortened. The geometric correlation by Kistenmacher *et al.* (1982) is 0.476 for neutral TCNQ, whereas for a negative radical with

Table 1
Selected absorption bands (cm^{-1}) of $TCNQ^{\delta-}$ in the infrared spectra of compounds **1**–**14**.

Assignment according to Lunelli & Pecile (1970). Overlapping bands, which could not be well resolved, are italic; w – weak; sh – shoulder.

Compound	C—H stretch	C—N stretch	C≡C ethyl stretch	C—H bend	C—CN stretch	NC—C—CN bend
1$_2$·Br·$(TCNQ)_2$	3053	2202, *2157*	1555, 1520	*1297*, 852	*1113*	482
2·$(TCNQ)_2$	3057	2202, *2177*	1563, 1516	*1336*, 859sh	1114	480
3·$(TCNQ)_2$	3047	2202, 2158	1555, 1513	*1341*sh, 837	*1115*	480
4·$(TCNQ)_2$	3047	2196, *2160*	1557, 1522	1323, 859	*1115*	480
5·$(TCNQ)_2$	3053	2200, *2171*sh	1563, 1515	*1330*, 822	*1113*	470
6·$(TCNQ)_2$	3057	2202, *2158*	1553, 1515	*1332*sh, 860	*1113*	483
7·$(TCNQ)_2$	3055	2202, *2167*	1557, 1517	*1332*, 856sh	*1114*	487
8·$(TCNQ)_2$	3059, 3035	2223w	1549	1338, 874	1121w	474
9·$(TCNQ)_4$	3062	2198, 2176	1561, 1526	1344, 841	1115	478
10·$(TCNQ)_3$	3051	2190, 2169	1564, 1516	1353, 862	*1113*sh	474
11$_2$·I·$(TCNQ)_2$	3053	2202, *2171*	1555, 1503	*1347*sh, 851	1104	480
12·$(TCNQ)_2$	3051	2200, *2178*	1553, 1520	*1295*, 859sh	*1113*	480
13·$(TCNQ)_2$	3057	2202, *2169*	1557, 1518	*1334*, 852w	*1111*	481
14·$(TCNQ)_2$	3057	2204, *2169*	1561, 1525	1359, 843	*1117*sh	482

a total charge of −1 it is 0.500. For the salts studied in this work with a formal charge on TCNQ of −1/2 it is 0.487 (4), corresponding to a charge of 0.44 (17) (Table 2). Although the average value is close to the expected one, large variance makes this geometric correlation quite unreliable. Similar results are obtained if the correlation is expanded to $(a + c)/(b + d)$. Average values of differences in bond lengths b–a and c–d for compounds with a formal charge on TCNQ of −1/2 studied in this work are 0.080 (10) and −0.034 (11) Å, respectively (Table 2). Again, the variances are too large to be reliable. Therefore, all these geometric correlations should be taken *cum grano salis*; as noted by Herbstein & Kapon (2008), 'it would be hazardous to base a distinction (for a single determination) on bond lengths *alone*'. Our conclusions for related semiquinone radicals were similar (Molčanov *et al.*, 2019*b*). The reason for this variance of molecular geometry can be attributed to the effect of crystal field and especially the strong, partially covalent pancake bonding between the radicals.

In the case of **10**·$(TCNQ)_3$, which comprises a pancake-bonded trimer with a formal charge of −2/3 [*i.e.* $(TCNQ)_3^{2-}$], the geometry indicates that the total charge of the central ring *B* is higher, −0.82, whereas the lateral rings *A* have a lower total charge of −0.45 (Table 2). Thus, the total charge of a trimer is −1.72, fairly close to the formal value of −2. Similar values have been found for similar trimers (Usov *et al.*, 1991). A more reliable assessment of total charge based on X-ray charge density was recently used in a study of a trimer of tetrachlorosemiquinone radicals with a formal charge of −2 (Molčanov *et al.*, 2018*b*), and it revealed similarly uneven distribution of the negative charge: the central ring has a higher total charge of −0.76, whereas the two lateral rings have a charge of −0.59. The total charge of that trimer was −1.94 (Molčanov *et al.*, 2018*b*). Accordingly, we may conclude that charge distribution in **10**·$(TCNQ)_3$ is similar.

Assignment of IR spectra in salts of $TCNQ^{\delta-}$ radicals is not straightforward owing to the presence of cation vibrations, which often overlap with bands of the $TCNQ^{\delta-}$ radical. However, stretching of the cyano group does not overlap with other bands, so it can be used as a rough estimate for the ionization state of $TCNQ^{\delta-}$ (Herbstein & Kapon, 2008): in the neutral molecule it is 2228 cm^{-1}, whereas in its mono anion there are two bands at 2194 and 2177 cm^{-1}. In the studied salts, there are two bands at about 2200 and 2160–2170 cm^{-1} (Table 1), of which the first is blue-shifted and the second is red-shifted compared with the fully negatively charged radical

Table 2
Estimated charge by geometric correlations.

Chemical bonds (labelled *a*, *b*, *c* and *d*) correspond to those in Fig. 1. RT – room temperature.

Ring	b–a	c–d	$c/(b + d)$	$(a + c)/(b + d)$	Est. charge†
1$_2$·Br·$(TCNQ)_2$	0.091	−0.044	0.483	0.988	0.31
2·$(TCNQ)_2$, 100 K	0.103	−0.055	0.478	0.993	0.10
2·$(TCNQ)_2$, RT	0.080	−0.031	0.488	0.989	0.48
3·$(TCNQ)_2$, *A*	0.083	−0.050	0.483	0.988	0.27
3·$(TCNQ)_2$, *B*	0.070	−0.024	0.490	0.989	0.59
4·$(TCNQ)_2$, *A*	0.088	−0.037	0.485	0.988	0.39
4·$(TCNQ)_2$, *B*	0.073	−0.018	0.492	0.986	0.68
5·$(TCNQ)_2$	0.088	−0.038	0.485	0.990	0.37
6·$(TCNQ)_2$, *A*	0.073	−0.029	0.488	0.992	0.50
6·$(TCNQ)_2$, *B*	0.087	−0.032	0.487	0.989	0.45
7·$(TCNQ)_2$, 100 K	0.085	−0.040	0.484	0.991	0.35
7·$(TCNQ)_2$, RT	0.082	−0.033	0.487	0.990	0.44
8·$(TCNQ)_2$, *A*	0.082	−0.030	0.488	0.987	0.50
8·$(TCNQ)_2$, *B*	0.080	−0.032	0.487	0.989	0.47
9·$(TCNQ)_4$, *A*	0.083	−0.036	0.486	0.990	0.41
9·$(TCNQ)_4$, *B*	0.075	−0.023	0.491	0.987	0.60
11$_2$·I·$(TCNQ)_2$, *A*	0.072	−0.024	0.490	0.989	0.58
11$_2$·I·$(TCNQ)_2$, *B*	0.066	−0.027	0.489	0.991	0.55
12·$(TCNQ)_2$, *A*	0.070	−0.028	0.489	0.989	0.55
12·$(TCNQ)_2$, *B*	0.053	−0.010	0.497	0.984	0.86
12·$(TCNQ)_2$, *C*	0.088	−0.050	0.481	0.992	0.22
13·$(TCNQ)_2$, 100 K, *A*	0.091	−0.054	0.480	0.991	0.17
13·$(TCNQ)_2$, 100 K, *B*	0.093	−0.051	0.481	0.991	0.20
13·$(TCNQ)_2$, RT	0.077	−0.027	0.489	0.989	0.54
14·$(TCNQ)_2$, 100 K	0.078	−0.034	0.487	0.987	0.48
14·$(TCNQ)_2$, RT	0.077	−0.027	0.488	0.991	0.52
10·$(TCNQ)_3$, *A*‡	0.084	−0.032	0.487	0.989	0.45
10·$(TCNQ)_3$, *B*‡	0.065	−0.008	0.496	0.986	0.82
Average	0.08 (1)	−0.03 (1)	0.487 (4)	0.989 (2)	0.4 (2)
TCNQ neutral§	0.096	−0.052	0.480	0.990	0
$TCNQ^-$§	0.068	−0.012	0.495	0.983	−1

† From $c/(b+d)$. ‡ Data for the trimer were not used to calculate the average. § Data obtained from the work by Herbstein & Kapon (2008).

Table 3
Geometric parameters of π interactions.

$\pi\cdots\pi$	Cg†···Cg (Å)	α‡	β§	Cg···plane(Cg2) (Å)	Offset (Å)	Symmetry operations on Cg2
1$_2$·Br·(TCNQ)$_2$						
C3→C11···C3→C11	5.166 (4)	0.0 (3)	52.1	3.176 (3)	4.075	$2-x, -2-y, 2-z$
C3→C11···C3→C11	4.974 (4)	0.0 (3)	48.1	3.324 (3)	3.701	$2-x, -1-y, 2-z$
C3→C11···C3→C11	3.720 (4)	0.0 (3)	32.7	3.129 (3)	2.011	$3-x, -2-y, 2-z$
N5→C17···C5→C17	4.906 (6)	0.0 (5)	41.0	3.700 (4)	3.222	$3-x, -1-y, 1-z$
2·(TCNQ)$_2$, 100 K						
C3→C11···C3→C11	3.680 (2)	0.00 (18)	32.9	3.090 (1)	1.998	$1-x, 1-y, 1-z$
C3→C11···C3→C11	5.014 (3)	6.63 (18)	48.0	3.013 (1)	3.728	$x, 1/2-y, -1/2+z$
C3→C11···C3→C11	5.014 (3)	6.63 (18)	53.1	3.353 (1)	4.008	$x, 1/2-y, 1/2+z$
2·(TCNQ)$_2$Q, RT						
C3→C11···C3→C11	3.719 (1)	0.02 (9)	32.5	3.1379 (8)	1.997	$1-x, 1-y, 1-z$
C3→C11···C3→C11	5.071 (1)	7.01 (9)	47.6	3.0665 (8)	3.744	$x, 1/2-y, -1/2+z$
C3→C11···C3→C11	5.071 (1)	7.01 (9)	52.8	3.4207 (8)	4.039	$x, 1/2-y, 1/2+z$
3·(TCNQ)$_2$						
C3A→C11A···C3B→C11B	3.759 (4)	1.3 (3)	32.5	3.157 (3)	2.022	$x, y, 1+z$
C3A→C11A···C3B→C11B	5.341 (4)	1.3 (3)	53.2	3.265 (3)	4.278	$1+x, -1+y, 1+z$
C3A→C11A···C3B→C11B	4.770 (4)	1.3 (3)	44.6	3.343 (3)	3.349	$1+x, y, 1+z$
C3B→C11B···C3A→C11A	4.770 (4)	1.3 (3)	45.5	3.397 (2)	3.402	$-1+x, y, -1+z$
C3B→C11B···C3A→C11A	5.340 (4)	1.3 (3)	52.3	3.197 (2)	4.226	$-1+x, 1+y, -1+z$
C3B→C11B···C3A→C11A	3.759 (4)	1.3 (3)	32.9	3.168 (2)	2.041	$x, y, -1+z$
4·(TCNQ)$_2$, 100 K						
C3A→C11A···C3A→C11A	3.8501 (7)	0.00 (5)	28.8	3.3732 (5)	1.856	$-x, 1-y, 1-z$
C3A→C11A···C3B→C11B	3.7472 (7)	2.57 (5)	33.2	3.1824 (5)	2.050	x, y, z
C3B→C11B···C3A→C11A	3.7471 (7)	2.57 (5)	31.9	3.1367 (4)	1.978	x, y, z
C3B→C11B···C3B→C11B	3.3476 (6)	0.03 (5)	20.8	3.1292 (4)	1.189	$1-x, 2-y, 1-z$
N5→C17···N5→C17	4.4886 (7)	0.00 (5)	31.8	3.8140 (4)	2.367	$1-x, 3-y, 2-z$
N5→C17···C20→C25	5.2401 (7)	61.04 (6)	47.0	3.8846 (4)	–	$-x, 3-y, 2-z$
C20→C25···N5→C17	5.2401 (7)	61.04 (6)	42.2	3.5715 (5)	–	$-x, 3-y, 2-z$
C20→C25···C20→C25	5.1280 (8)	0.00 (7)	50.8	3.240 (6)	3.975	$-x, 2-y, 2-z$
4·(TCNQ)$_2$, RT						
C3A→C11A···C3A→C11A	3.9170 (8)	0.00 (7)	29.5	3.4101 (6)	1.927	$-x, 1-y, 1-z$
C3A→C11A···C3B→C11B	3.8016 (8)	2.04 (6)	32.8	3.2338 (6)	2.058	x, y, z
C3B→C11B···C3A→C11A	3.8017 (8)	2.04 (6)	31.7	3.1968(5)	1.999	x, y, z
C3B→C11B···C3B→C11B	3.4907 (7)	0.03 (6)	22.5	3.2250 (5)	1.336	$1-x, 2-y, 1-z$
N5→C17···N5→C17	4.5411 (8)	0.00 (7)	30.9	3.8977 (6)	2.330	$1-x, 3-y, 2-z$
N5→C17···C20→C25	5.255 (1)	61.99 (9)	46.5	4.0163 (5)		$-x, 3-y, 2-z$
C20→C25···N5→C17	5.255 (1)	61.99 (9)	40.2	3.6197 (9)		$-x, 3-y, 2-z$
C20→C25···C20→C25	5.364 (1)	0.0 (1)	51.9	3.3067 (9)	4.224	$-x, 2-y, 2-z$
5·(TCNQ)$_2$						
C3→C11···C3→C11	3.798 (1)	0.02 (9)	32.1	3.2167 (8)	2.020	$1-x, 1-y, 2-z$
6·(TCNQ)$_2$						
C3A→C11A···C3B→C11B	5.033 (4)	0.5 (3)	51.0	3.145 (3)	3.910	x, y, z
C3A→C11A···C3B→C11B	5.082 (4)	0.5 (3)	50.3	3.271 (3)	3.908	$x, 1+y, z$
C3A→C11A···C3B→C11B	3.727 (4)	0.5 (3)	33.0	3.124 (3)	2.030	$1+x, y, z$
C3B→C11B···C3A→C11A	3.726 (4)	0.5 (3)	33.1	3.125 (3)	2.032	$-1+x, y, z$
C3B→C11B···C3A→C11A	5.082 (4)	0.5 (3)	49.9	3.249 (3)	3.889	$x, -1+y, z$
C3B→C11B···C3A→C11A	5.034 (4)	0.5 (3)	51.3	3.169 (3)	3.930	x, y, z
7·(TCNQ)$_2$, 100 K						
C3→C11···C3→C11	3.6872 (9)	0.03 (7)	33.2	3.0866 (6)	2.017	$-x, 2-y, -z$
C3→C11···C3→C11	5.1357 (9)	0.03 (7)	52.2	3.1470 (6)	4.059	$1-x, 1-y, -z$
C3→C11···C3→C11	4.9180 (9)	0.03 (7)	49.9	3.1696 (6)	3.760	$1-x, 2-y, -z$
7·(TCNQ)$_2$, RT						
C3→C11···C3→C11	3.7390 (9)	0.02 (7)	32.7	3.1455 (6)	2.021	$-x, -y, 1-z$
C3→C11···C3→C11	5.0008 (9)	0.02 (7)	49.7	3.2335 (6)	3.815	$1-x, -y, 1-z$
C3→C11···C3→C11	5.1723 (9)	0.02 (7)	51.3	3.2310 (6)	4.039	$1-x, 1-y, 1-z$
8·(TCNQ)$_2$						
C3A→C11A···C3A→C11A	3.771 (1)	0.(1)	24.9	3.4198 (9)	1.590	$2-x, 1-y, 2-z$
C3A→C11A···C3B→C11B	3.685 (1)	1.6 (1)	32.5	3.1408 (9)	1.978	$x, y, 1+z$
C3B→C11B···C3A→C11A	3.685 (1)	1.6 (1)	31.5	3.1089 (9)	1.927	$x, y, -1+z$
C3B→C11B···C3B→C11B	3.718 (1)	0.0 (1)	28.0	3.2831 (9)	1.744	$1-x, -y, -z$
9·(TCNQ)$_2$						
C3A→C11A···C3A→C11A	5.1343 (7)	16.73 (6)	43.1	2.8125 (5)	3.509	$x, 1/2-y, 1/2+z$
C3A→C11A···C3B→C11B	3.7304 (7)	2.08 (6)	31.6	3.1874 (5)	1.956	x, y, z
C3B→C11B···C3A→C11A	3.7304 (7)	2.08 (6)	31.3	3.1765 (5)	1.938	x, y, z
C3B→C11B···C3B→C11B	3.7423 (7)	0.00 (6)	31.9	3.1785 (5)	1.975	$1-x, 1-y, -z$
10·(TCNQ)$_3$						
C3A→C11A···C3A→C11A	4.907 (1)	0.03 (9)	47.0	3.3459 (7)	3.590	$-x, 3-y, 1-z$
C3A→C11A···C3A→C11A	5.181 (1)	0.03 (9)	54.6	3.0009 (7)	4.224	$1-x, 3-y, 1-z$
C3A→C11A···C3B→C5B_a	3.646 (1)	1.23 (8)	33.9	3.0362 (7)	2.036	x, y, z
C3B→C5B_a···C3A→C11A	3.646 (1)	1.23 (8)	33.6	3.0251 (7)	2.019	x, y, z

Table 3 (continued)

$\pi\cdots\pi$	Cg†···Cg (Å)	α‡	β§	Cg···plane(Cg2) (Å)	Offset (Å)	Symmetry operations on Cg2
11$_2$·I·(TCNQ)$_2$						
C3A→C11A···C3A→C11A	3.638 (2)	0.0 (2)	31.4	3.105 (1)	1.896	$1-x, 2-y, 2-z$
C3A→C11A···C3B→C11B	5.255 (2)	7.2 (2)	59.2	3.173 (1)	4.515	x, y, z
C3A→C11A···C3B→C11B	4.592 (2)	7.2 (2)	41.5	3.104 (1)	3.043	$1+x, y, z$
C3B→C11B···C3A→C11A	4.592 (2)	7.2 (2)	47.5	3.438 (1)	3.383	$-1+x, y, z$
C3B→C11B···C3A→C11A	5.255 (2)	7.2 (2)	52.9	2.689 (1)	4.189	x, y, z
C3B→C11B···C3B→C11B	3.688 (2)	0.0 (2)	33.4	3.079 (1)	2.029	$-x, 3-y, 2-z$
N5→C17···N5→C17	4.622 (2)	0.0 (2)	36.3	3.725 (1)	2.736	$-x, 2-y, 1-z$
12·(TCNQ)$_2$						
C3A→C11A···C3A→C11A	4.017 (2)	0.0 (1)	33.3	3.357 (1)	2.207	$1-x, 1-y, 1-z$
C3A→C11A···C3A→C11A	3.694 (2)	0.0 (1)	33.0	3.098 (1)	2.012	$2-x, 1-y, 1-z$
C3B→C10B_a···C3C→C10C_b	4.240 (2)	1.1 (1)	39.9	3.307 (1)	2.718	$-1+x, -1+y, z$
C3C→C10C_b···C3B→C10B_a	4.240 (2)	1.1 (1)	38.7	3.254 (1)	2.653	x, y, z
13·(TCNQ)$_2$, 100 K						
C3A→C11A···C3A→C11A	3.689 (1)	0.02 (9)	33.0	3.0946 (8)	2.008	$1-x, 2-y, 2-z$
C3A→C11A···C3B→C11B	5.064 (1)	8.23 (9)	47.3	2.9296 (8)	3.719	$-x, 1-y, 1-z$
C3A→C11A···C3B→C11B	4.935 (1)	8.23 (9)	53.9	3.3783 (8)	3.990	$1-x, 1-y, 1-z$
C3B→C11B···C3A→C11A	5.064 (1)	8.23 (9)	54.7	3.4366 (8)	4.130	$-x, 1-y, 1-z$
C3B→C11B···C3A→C11A	4.935 (1)	8.23 (9)	46.8	2.9043 (8)	3.597	$1-x, 1-y, 1-z$
C3B→C11B···C3B→C11B	3.689 (1)	0.02 (9)	33.1	3.0914 (8)	2.013	$-x, 1-y, -z$
13·(TCNQ)$_2$, RT						
C1→C6···C1→C6	3.723 (2)	0.0 (1)	32.5	3.139 (1)	2.002	$-x, -y, 1-z$
C1→C6···C1→C6	5.017 (2)	0.0 (1)	49.2	3.277 (1)	3.798	$1-x, -y, 1-z$
C1→C6···C1→C6	5.082 (2)	0.0 (1)	51.2	3.186 (1)	3.959	$1-x, 1-y, 1-z$
14·(TCNQ)$_2$, 100 K						
C3→C11···C3→C11	4.771 (2)	0.0 (2)	46.3	3.297 (1)	3.449	$-x, 1-y, 1-z$
C3→C11···C3→C11	5.265 (2)	0.0 (2)	53.1	3.162 (1)	4.210	$-x, 2-y, 1-z$
C3→C11···C3→C11	3.687 (2)	0.0 (2)	32.9	3.097 (1)	2.000	$1-x, 1-y, 1-z$
14·(TCNQ)$_2$, RT						
C3→C11···C3→C11	4.742 (2)	0.0 (1)	44.4	3.390 (1)	3.316	$-x, 1-y, 1-z$
C3→C11···C3→C11	5.423 (2)	0.0 (1)	53.7	3.207 (1)	4.373	$-x, 2-y, 1-z$
C3→C11···C3→C11	3.738 (2)	0.0 (1)	32.4	3.155 (1)	2.004	$1-x, 1-y, 1-z$

† Cg – centroid of the aromatic ring. ‡ α – angle between planes of two interacting rings. § β – angle between Cg···Cg line and normal to the plane of the first interacting ring.

anion, indicating a partial radical nature. The ethyl C=C stretching band is red-shifted compared with the neutral TCNQ$^{\delta-}$ by 20–25 cm^{-1}, indicating weaker C=C bonds due to enhanced delocalization of π-electrons (Table 1).

2.2. Crystal packing and multicentre bonding

In all the studied crystal structures the dominant motif is the stacking of TCNQ$^{\delta-}$ radical anions, with a secondary motif of weak C—H···N hydrogen bonding between dimers (or oligomers) of the radicals. These two motifs create 2D-layered arrays of TCNQ$^{\delta-}$ radicals, which we discuss below. In all cases there are separate layers of radicals and cations, connected by C—H···N hydrogen bonds. Geometric parameters of π-stacking contacts are given in Table 3; note that interplanar distances corresponding to pancake bonding (*i.e.* those within the oligomers) are rather short (typically <3.25 Å), whereas those between the oligomers are longer (mostly exceeding 3.3 Å). However, these differences are much less pronounced than in semiquinones, where inter-dimer distances usually exceed 3.4 Å (Molčanov *et al.*, 2016; 2018*a*; 2019*b*,*c*).

A pancake-bonded dimer of partially charged TCNQ$^{\delta-}$ moieties, $(TCNQ)_2^{-}$, as a main unit is present in **1**$_2$·Br·(TCNQ)$_2$, **2**·(TCNQ)$_2$, **3**·(TCNQ)$_2$, **5**·(TCNQ)$_2$, **6**·(TCNQ)$_2$, **7**·(TCNQ)$_2$, **8**·(TCNQ)$_2$, **11**$_2$·I·(TCNQ)$_2$, **12**·(TCNQ)$_2$, **13**·(TCNQ)$_2$ and **14**·(TCNQ)$_2$. In **10**·(TCNQ)$_3$ it is the trimer $(TCNQ)_3^{2-}$, and in **4**·(TCNQ)$_2$ and **9**·(TCNQ)$_4$ it is the tetramer $(TCNQ)_4^{2-}$. Dimers are common in almost all planar radicals, semiquinones (Molčanov *et al.*, 2018*a*; 2019*b*,*c*; Molčanov & Kojić-Prodić, 2019), various diazolyls (Lekin *et al.*, 2010; Yu *et al.*, 2011, 2012; Melen *et al.*, 2016; Nikolayenko *et al.*, 2017; Beldjoudi *et al.*, 2019) *etc*. They typically involve a pair of radicals, each having a single unpaired electron; thus the intermolecular HOMO is filled by a pair of electrons and the multicentre bond order is 1 (Mou & Kertesz, 2017; Molčanov *et al.*, 2018*b*, 2019*a*). Such structures are therefore diamagnetic. However, in the present case of TCNQ$^{\delta-}$, stoichiometry (and molecular geometry, see above) indicates that their charge is −1/2, so a dimer contains a single unpaired electron, $(TCNQ)_2^{-}$. Thus, the muticentre bond order is 1/2 (Mou & Kertesz, 2017; Molčanov *et al.*, 2018*b*) and the single electron remains unpaired.

Trimers in **10**·(TCNQ)$_3$ are similar to those observed in semiquinones (Molčanov *et al.*, 2018*b*, 2019*c*; Molčanov & Kojić-Prodić, 2019), sharing two electrons per three radicals, implying a multicentre bond order of <0.71 (Molčanov *et al.*, 2018*b*). The two electrons occupying the HOMO of the $(TCNQ)_3^{2-}$ group are paired and the ground state is antiferromagnetic.

Tetramers $(TCNQ)_4^{2-}$ in **4**·(TCNQ)$_2$ and **9**·(TCNQ)$_4$ involve four TCNQ$^{\delta-}$ radicals with a formal charge of −1/2, meaning two electrons occupy the HOMO. Therefore, the multicentre bond order is about 1/2 (Mou & Kertesz, 2017;

Molčanov *et al.*, 2018*b*), since a pair of electrons is shared by four TCNQ rings.

The dimers, trimers and tetramers are stacked by somewhat weaker π-interactions (Molčanov & Kojić-Prodić, 2019; Molčanov *et al.*, 2019*c*) and laterally connected by C—H···N hydrogen bonds (Table 4, Fig. 2) into 2D arrays. The cyano group of the $TCNQ^{\delta-}$ radical is a strong acceptor, and the proton-donating capability of the C—H group is barely

Table 4
Geometric parameters of hydrogen bonds.

	D—H (Å)	H···*A* (Å)	*D*···*A* (Å)	*D*—H···*A* (°)	Symmetry operations on *A*
1$_2$·Br·(TCNQ)$_2$					
C16—H16···N4	0.93	2.48	3.39 (2)	167	$x, 1+y, z$
C18—H18A···N4	0.96	2.59	3.12 (1)	115	$1+x, y, z$
2·(TCNQ)$_2$, 100 K					
C4—H4···N3	0.93	2.59	3.266 (7)	130	$x, y, -1+z$
C11—H11···N2	0.93	2.57	3.248 (7)	130	$x, y, 1+z$
C16—H16···N1	0.93	2.53	3.42 (1)	161	$-1+x, -1/2-y, 1/2+z$
3·(TCNQ)$_2$					
C4A—H4A···N3A	0.93	2.59	3.30 (1)	134	$x, 1+y, z$
C4B—H4B···N3B	0.93	2.54	3.28 (1)	136	$x, 1+y, z$
C11A—H11A···N2A	0.93	2.56	3.29 (1)	135	$x, -1+y, z$
C11B—H11B···N2B	0.93	2.61	3.36 (1)	138	$x, -1+y, z$
C13—H13···N1A	0.93	2.31	3.24 (1)	177	$-1+x, 1+y, -1+z$
C15—H15···N4B	0.93	2.61	3.35 (2)	136	$1+x, y, 1+z$
C18—H18A···N4B	0.96	2.59	3.55 (2)	179	$x, 1+y, 1+z$
4·(TCNQ)$_2$					
C5A—H5A···N2B	0.93	2.60	3.331 (2)	136	$-x, 2-y, 1-z$
C11A—H11A···N3B	0.93	2.48	3.282 (2)	145	$1-x, 1-y, 1-z$
C14A—H14A···N1B	0.93	2.45	3.170 (2)	134	$x, 1+y, 1+z$
C16—H16···N2B	0.93	2.54	3.457 (2)	168	x, y, z
C18—H18C···N4A	0.96	2.49	3.305 (2)	143	$x, 1+y, z$
C22—H22···N1B	0.93	2.52	3.374 (3)	153	$-x, 2-y, 1-z$
6·(TCNQ)$_2$					
C13—H13···N4A	0.93	2.55	3.27 (1)	135	$x, y, 1+z$
C16—H16···N1B	0.93	2.50	3.29 (1)	143	x, y, z
C17—H17···N1A	0.93	2.59	3.48 (2)	143	$-1+x, y, z$
7·(TCNQ)$_2$, 100 K					
C13—H13···N1	0.93	2.54	3.242 (2)	133	$1-x, 1-y, 1-z$
7·(TCNQ)$_2$, RT					
N6—H16A···N1	1.00 (4)	2.56 (4)	3.316 (4)	133 (3)	$-1+x, y, z$
C13—H13···N1	0.93	2.56	3.302 (3)	137	$1-x, 1-y, 2-z$
8·(TCNQ)$_2$					
C11A—H11A···N1A	0.93	2.57	3.250 (3)	130	$-1+x, y, z$
C13—H13···N2B	0.93	2.46	3.220 (3)	139	$x, 1+y, 1+z$
C17—H17···N3A	0.93	2.53	3.284 (3)	139	$-1+x, y, -1+z$
C18—H18B···N4B	0.97	2.62	3.366 (3)	134	$-x, 1-y, -z$
9·(TCNQ)$_4$					
C13—H13···N2A	0.93	2.43	3.353 (2)	172	$1-x, 1-y, 1-z$
C1—H1···N2B	0.93	2.42	3.332 (2)	167	$1-x, 1-y, 1-z$
C17—H17···N3B	0.93	2.40	3.239 (2)	150	$-x, 1-y, -z$
10·(TCNQ)$_3$					
C13—H13···N3A	0.93	2.54	3.447 (3)	165	$-x, 2-y, 2-z$
C14—H14···N3B	0.93	2.34	3.116 (2)	140	$-1+x, y, 1+z$
C17—H17···N2A	0.93	2.55	3.250 (2)	132	$1-x, 3-y, 1-z$
11$_2$·I·(TCNQ)$_2$					
C5A—H5A···N4A	0.93	2.60	3.341 (4)	137	$1+x, y, z$
C5B—H5B···N4B	0.93	2.51	3.267 (4)	139	$1+x, y, z$
C10A—H10A···N1A	0.93	2.57	3.277 (4)	133	$-1+x, y, z$
C10B—H10B···N1B	0.93	2.53	3.285 (4)	139	$-1+x, y, z$
C13B—H13B···I1	0.93	2.95	3.848 (4)	164	$2-x, 1-y, 1-z$
C15B—H15B···N2A	0.93	2.60	3.332 (6)	136	$2-x, 2-y, 1-z$
C17A—H17A···N2A	0.93	2.59	3.495 (5)	164	$-1+x, y, z$
C17B—H17B···N2B	0.93	2.54	3.225 (5)	131	$2-x, 2-y, 1-z$
C18B—H18B···I1	0.96	3.05	3.784 (4)	134	$-1+x, y, z$
C18B—H18D···N3B	0.96	2.54	3.484 (5)	166	$2+x, -1+y, -1+z$
12·(TCNQ)$_2$					
C4C—H4C···N1C	0.93	2.62	3.244 (3)	125	$2-x, -y, -z$
C13—H13···N3C	0.93	2.51	3.375 (4)	155	$x, -1+y, z$
13·(TCNQ)$_2$, 100 K					
C4A—H4A···N3A	0.93	2.62	3.318 (3)	132	$1+x, y, z$
C4B—H4B···N3B	0.93	2.60	3.272 (3)	130	$1+x, y, z$
C11B—H11B···N2B	0.93	2.60	3.271 (3)	129	$-1+x, y, z$
C13—H13···N1B	0.93	2.44	3.356 (3)	170	x, y, z
C14—H14···N4B	0.93	2.49	3.316 (3)	148	$-x, 1-y, -z$

Table 4 (continued)

	D—H (Å)	H···A (Å)	D···A (Å)	D—H···A (°)	Symmetry operations on A
C15—H15···N4B	0.93	2.56	3.305 (4)	137	$1 + x, 1 + y, 1 + z$
C16—H16···N1A	0.93	2.60	3.362 (4)	139	$2 - x, 2 - y, 2 - z$
C17—H17···N4A	0.93	2.61	3.446 (3)	150	$1 + x, y, z$
14·(TCNQ)$_2$, 100 K					
C5—H5···N4	0.93	2.56	3.270 (5)	134	$x, 1 + y, z$
C10—H10···N1	0.93	2.60	3.317 (5)	134	$x, -1 + y, z$
C15—H15···N3	0.93	2.60	3.338 (6)	137	$1 + x, y, z$
14·(TCNQ)$_2$, RT					
C5—H5···N4	0.93	2.59	3.299 (4)	134	$x, 1 + y, z$

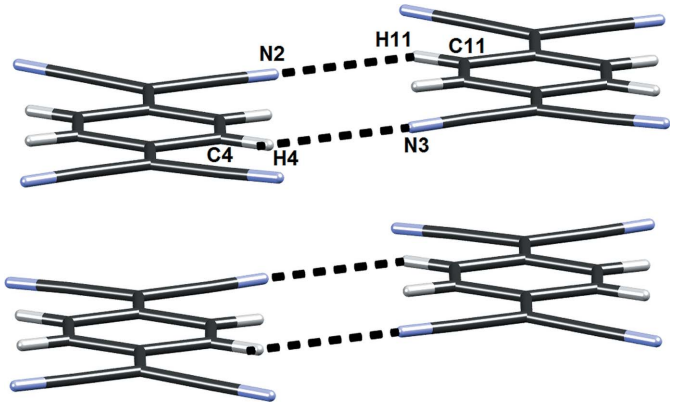

Figure 2
Typical lateral connection between pancake-bonded pairs in **1**$_2$·Br·(TCNQ)$_2$, involving two pairs of C—H···N hydrogen bonds.

affected by a partial negative charge. In addition, a lateral contact between two radicals involves two hydrogen bonds, so the interaction is fairly strong. Therefore, the motif shown in Fig. 2 is observed in all structures. All the studied structures involve alternating layers of anions and cations (Fig. 3), and these layers are connected by C—H···N hydrogen bonds with the cation acting as a weak donor and the cyano groups of TCNQ$^{\delta-}$ acting as acceptors (Fig. 4). Typically, there are only dispersion interactions between the cations. Stacking between aromatic cations was observed in the compounds **1**$_2$·Br·(TCNQ)$_2$, **4**·(TCNQ)$_2$ and **11**$_2$·I·(TCNQ)$_2$, but it is a much weaker interaction with interplanar distances exceeding 3.6 Å. Such geometry is common for aromatic π-interactions (Molčanov & Kojić-Prodić, 2019; Molčanov *et al.*, 2019*c*).

The most common type of 2D arrangement is a 'brick wall' pattern of pancake-bonded dimers, which is found in

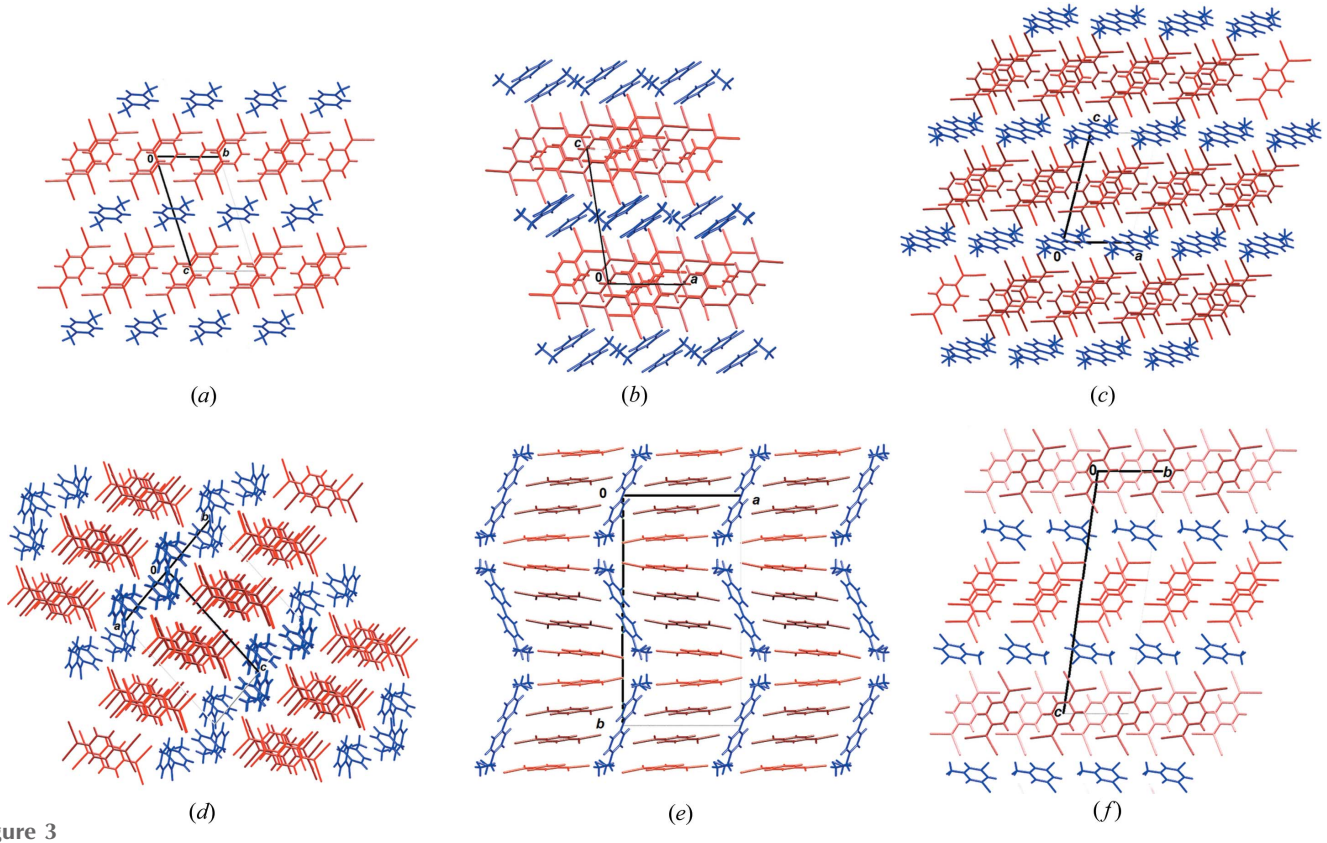

Figure 3
Crystal packings showing layers of TCNQ$^{\delta-}$ moieties (red) and cations (blue) of (*a*) **7**·(TCNQ)$_2$, (*b*) **8**·(TCNQ)$_2$, (*c*) **10**·(TCNQ)$_3$, (*d*) **4**·(TCNQ)$_2$, (*e*) **9**·(TCNQ)$_4$ and (*f*) **12**·(TCNQ)$_2$. Symmetry-independent moieties are shown in lighter and darker shades.

$\mathbf{1}_2$·Br·$(TCNQ)_2$, $\mathbf{2}$·$(TCNQ)_2$, $\mathbf{3}$·$(TCNQ)_2$, $\mathbf{6}$·$(TCNQ)_2$, $\mathbf{7}$·$(TCNQ)_2$ $\mathbf{11}_2$·I·$(TCNQ)_2$, $\mathbf{12}$·$(TCNQ)_2$, $\mathbf{13}$·$(TCNQ)_2$ and $\mathbf{14}$·$(TCNQ)_2$ [Figs. 4(*a*) and S4–S17]. A similar pattern, although with fewer hydrogen bonds, is also present in $\mathbf{5}$·$(TCNQ)_2$. In $\mathbf{8}$·$(TCNQ)_2$ the pancake-bonded dimers form hydrogen-bonded chains parallel to [001], which are stacked on top of one another [Fig. 4(*b*)]. Brick-wall patterns are also formed by trimers in $\mathbf{10}$·$(TCNQ)_3$ [Fig. 4(*c*)] and tetramers in $\mathbf{4}$·$(TCNQ)_2$ [Fig. 4(*d*)]. Tetramers in $\mathbf{9}$·$(TCNQ)_4$ are laterally connected into chains parallel to [001], and are inclined by *ca* 20° towards the *b* axis. The contiguous chains are inclined in opposite directions, resulting in a herringbone-like pattern [Fig. 4(*e*)]. Interactions between the chains are very weak.

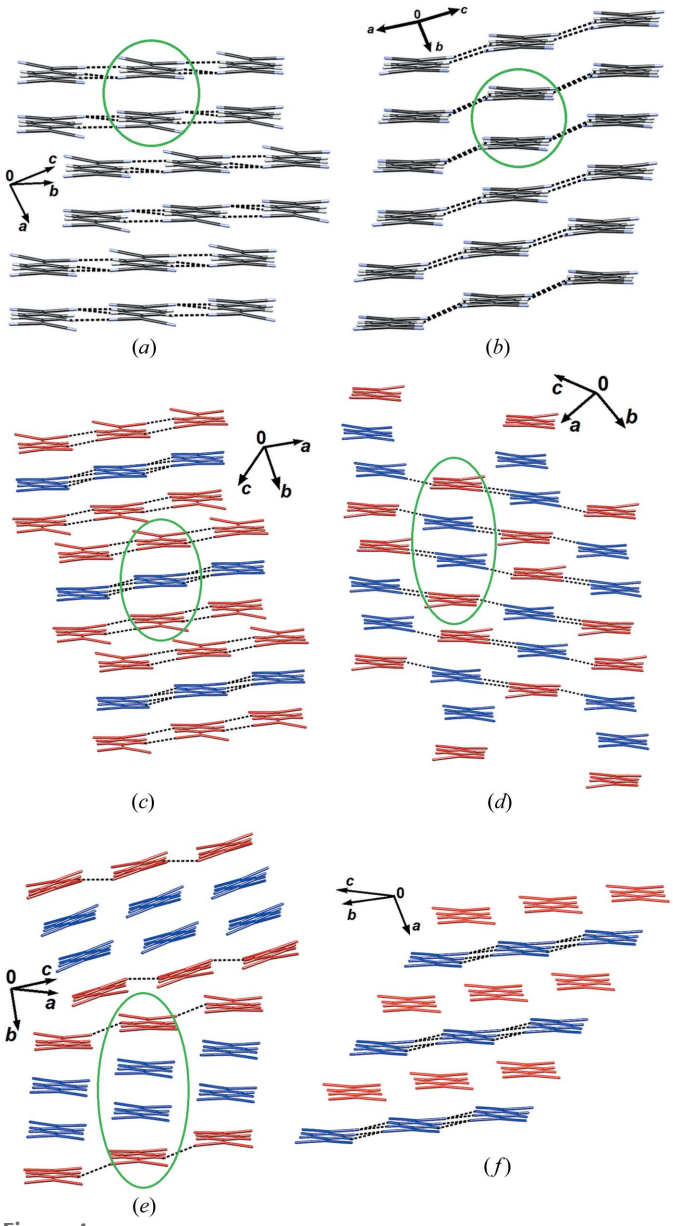

Figure 4
Different types of layers of $TCNQ^{\delta-}$ radicals observed in the compounds studied: (*a*) 'brick wall' array of pancake-bonded dimers in $\mathbf{7}$·$(TCNQ)_2$, (*b*) stacking of parallel hydrogen-bonded chains in $\mathbf{8}$·$(TCNQ)_2$, (*c*) brick-wall array of pancake-bonded trimers in $\mathbf{10}$·$(TCNQ)_3$ (*A* are red and *B* are blue), (*d*) brick wall array of pancake-bonded tetramers in $\mathbf{4}$·$(TCNQ)_2$ (*A* are red and *B* are blue), (*e*) herringbone-like array of pancake-bonded tetramers in $\mathbf{9}$·$(TCNQ)_4$ (*A* are red and *B* are blue) and (*f*) 2D array formed by stacks of equidistant radicals in $\mathbf{12}$·$(TCNQ)_2$ (*B* are red and *C* are blue). Individual dimers, trimers and tetramers are highlighted in green; hydrogen bonds are shown as black dotted lines.

The unique crystal packing in the series studied is the structure of $\mathbf{12}$·$(TCNQ)_2$ which comprises three symmetry-independent $TCNQ^{\delta-}$ radicals (labelled *A*, *B* and *C*), each with a formal charge of −1/2. Molecule *A*, which is located in a general position, forms a 2D brick-wall pattern of pancake bonded dimers, identical to those described above [Fig. 4(*a*)]. Centrosymmetric anions *B* and *C* form equidistant stacks with alternating rings (...*BCBC*...) extending in the direction [100]. Hydrogen bonds (C—H···N) between the *C* rings connect the stacks into layers parallel to (001) [Fig. 4(*f*)]. The overall crystal packing exhibits alternating layers: anions *A*...cations ...anions *B*/*C*...cations...anions *A*... (Fig. S15 of the supporting information).

In some structures intermolecular halogen bonding is present. The crystal packing of $\mathbf{1}_2$·Br·$(TCNQ)_2$ involves a bromide anion located at an inversion centre (p.p. 0.5) which is connected to two cations of $\mathbf{1}$ by a pair of symmetry-related Br···Br halogen bonds of 3.356 Å (Fig. 5). Similarly, in $\mathbf{11}_2$·I·$(TCNQ)_2$, an iodide anion forms a pair of Br···I halogen bonds of 3.556 and 3.662 Å. In both structures the halogen bonds are (approximately) collinear [180° in $\mathbf{1}_2$·Br·$(TCNQ)_2$ and at *ca* 161° in $\mathbf{11}_2$·I·$(TCNQ)_2$]. In addition, the halide also acts as an acceptor of several C—H···Br (C—H···I) hydrogen bonding contacts, as is usually observed in halogenopyridine halogenides (Grebe *et al.*, 1999; Logothetis *et al.*, 2004; Caballero *et al.*, 2012; Fotović & Stilinović, 2020). Halogen bonding is also present in $\mathbf{3}$·$(TCNQ)_2$, $\mathbf{6}$·$(TCNQ)_2$, $\mathbf{8}$·$(TCNQ)_2$ and $\mathbf{12}$·$(TCNQ)_2$ where cyano groups of $TCNQ^{\delta-}$ anions act as halogen bond acceptors. However, there is a significant difference between the halogen bonds formed by the iodopyridinium cations [in $\mathbf{3}$·$(TCNQ)_2$ and $\mathbf{6}$·$(TCNQ)_2$] and the dibromopyridinium cations [in $\mathbf{8}$·$(TCNQ)_2$ and $\mathbf{12}$·$(TCNQ)_2$]. The iodopyridinium cations form I···N halogen bonds [of 3.322 Å in $\mathbf{3}$·$(TCNQ)_2$ and 3.172 Å in $\mathbf{6}$·$(TCNQ)_2$] with the cyano nitrogen lone pair, whereas the dibromopyridinium cations form halogen bonds orthogonal to the cyano group (*i.e.* with the π-electrons of the cyano group). Note that both bond geometries have been observed in halogen-bonded structures of coordination complexes of cyanide ligands (Mínguez Espallargas *et al.*, 2009; Ormond-Prout *et al.*, 2012; Jakupec *et al.*, 2020) with a formal negative charge.

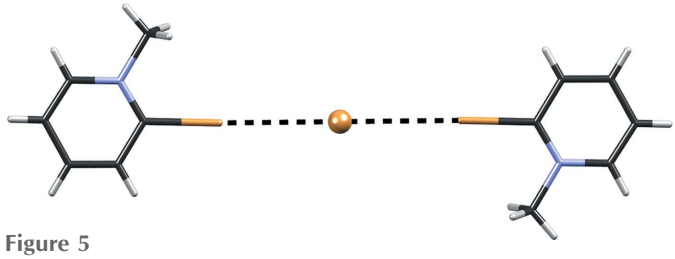

Figure 5
Bromide anion held by a pair of symmetry-related halogen bonds Br···Br in $\mathbf{1}_2$·Br·$(TCNQ)_2$.

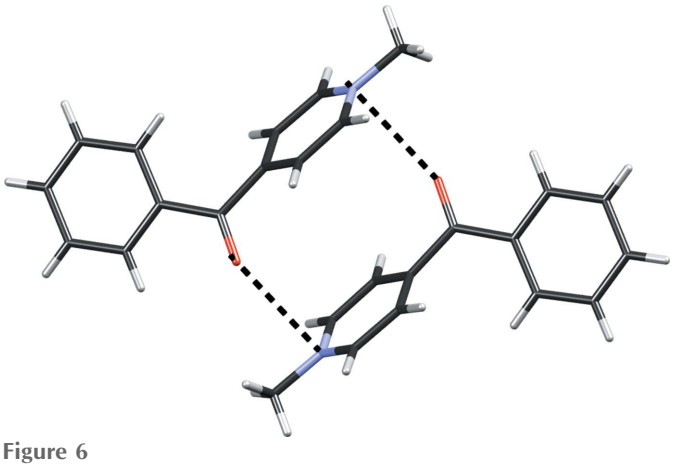

Figure 6
Dimer of cations of **4** in **4**·(TCNQ)$_2$ formed by π–hole interactions (shown as dashed lines) and π-stacking of pyridyl rings enhanced by antiparallel local dipoles.

In **4**·(TCNQ)$_2$ the cations form a dimer through a pair of π–hole interactions involving a carbonyl group and pyridinium ring; in addition the pyridinium rings stack, and this interaction is enhanced by antiparallel local dipoles (Fig. 6). π–Hole interactions are also present in **8**·(TCNQ)$_2$, between a cyano group from the TCNQ$^{\delta-}$ molecule *B* and the pyridinium ring of the cation, and also in **12**·(TCNQ)$_2$ between the iodide anion and pyridinium ring of the cation.

2.3. Correlation of electrical conductivity and crystal packing

Impedance spectroscopy measurements of selected compounds: **1**$_2$·Br·(TCNQ)$_2$, **4**·(TCNQ)$_2$, **6**·(TCNQ)$_2$, **8**·(TCNQ)$_2$, **9**·(TCNQ)$_4$, **10**·(TCNQ)$_3$ and **12**·(TCNQ)$_2$ showed that conductivity isotherms of all samples are frequency-independent (corresponding to DC conductivity) over a wide range of frequencies. Fig. 7 shows the conductivity spectra of **10**·(TCNQ)$_3$ as typical spectra for all measured compounds. The observed behaviour is typical for electronically conducting materials and indicates fast electron transport (Austin, 1970; Morimoto *et al.*, 2019; Renka *et al.*, 2020).

For all measured compounds, the DC conductivity exhibits Arrhenius temperature dependence and hence has a characteristic activation energy, see Fig. 8. The activation energy for DC conductivity (E_{DC}) for each compound was determined from the slope log(σ_{DC}) versus 1000/T using the equation $\sigma_{DC}T = \sigma_0\exp(-E_{DC}/k_BT)$, where σ_{DC} is the conductivity, σ_0 is the pre-exponential factor, E_{DC} is the activation energy, k_B is the Boltzmann constant and T is the temperature (K). The DC conductivities at 293 K and the determined activation energies (E_{DC}) for all compounds are listed in Table 5.

The electrical conductivities are higher than those observed for similar salts of semiquinones (Molčanov *et al.*, 2016; 2018*a*), whose conductivities are below 10^{-6} (Ω cm^{-1}) and are among the highest for ionic radicals. The phenomenon can be attributed to the shorter interplanar distance between oligomers (Table 3) and probably with a partial radical character of

Table 5
Electrical conductivity (σ_{DC}) and activation energy for conductivity (E_{DC}) of selected compounds.

Compound	σ_{DC} (Ω cm)$^{-1}$ at 20°C	E_{DC} (eV)
1$_2$·Br·(TCNQ)$_2$	2.36 × 10^{-7}	0.22
4·(TCNQ)$_2$	4.15 × 10^{-6}	0.26
6·(TCNQ)$_2$	3.35 × 10^{-6}	0.12
8·(TCNQ)$_2$	5.29 × 10^{-5}	0.21
9·(TCNQ)$_4$	2.44 × 10^{-2}	0.05
10·(TCNQ)$_3$	1.91 × 10^{-4}	0.22
12·(TCNQ)$_2$	5.07 × 10^{-5}	0.19

TCNQ$^{\delta-}$. The lowest-conducting compound **1**$_2$·Br·(TCNQ)$_2$ contains bromide anions as well as TCNQ$^{\delta-}$. The radical dimers are arranged in a 2D brick wall-like array (Fig. S4), but the interplanar distances between the dimers are only 0.05 and 0.10 Å longer than the distances within the dimer. These small differences imply that the electrons can jump between the dimers.

The next-lowest conducting compound is **4**·(TCNQ)$_2$, which comprises a 'brick wall' pattern of tetramers; a relatively large inter-tetramer separation of 3.3732 (5) Å indicates a relatively high energy barrier for electrons jumping between the tetra-

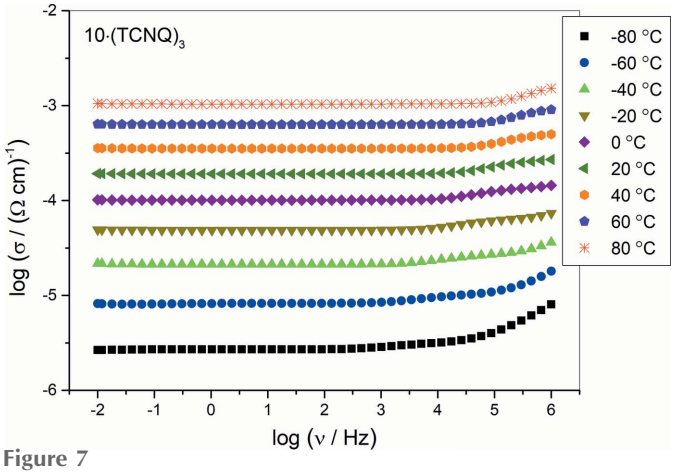

Figure 7
Electrical conductivity spectra of **10**·(TCNQ)$_3$ at different temperatures.

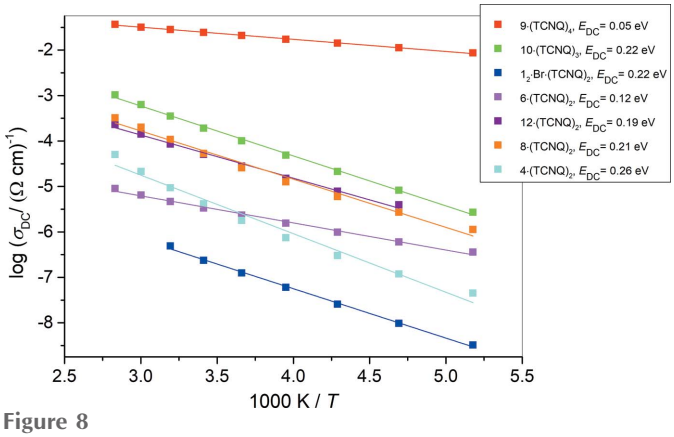

Figure 8
Electrical conductivity as a function of reciprocal temperature for all measured compounds. Solid lines represent the least-squares linear fit to the experimental data (full symbols).

Table 6
Spin counting results.

Sample	M_r	N_{mol}	N_{spin}	N_{spin}/N_{mol}	Formal charge
$\mathbf{1}_2$·Br·$(TCNQ)_2$	461.15	5.2584e+18	2.4524e+18	0.46±0.09	1
4·$(TCNQ)_2$	606.61	1.8107e+18	5.6066e+17	0.31±0.06	1
6·$(TCNQ)_2$	746.39	2.3884e+18	2.2957e+18	0.96±0.19	1
8·$(TCNQ)_2$	746.39	2.3884e+18	9.6413e+14	0.0004±0.00008	1
9·$(TCNQ)_4$	662.68	1.0416e+18	1.9589e+18	1.88±0.38	2
10·$(TCNQ)_3$	594.63	1.2618e+18	7.2700e+16	0.06±0.01	2
12·$(TCNQ)_2$	660.30	1.1908e+18	1.0446e+18	0.87±0.18	1

mers. The following four salts **6**·$(TCNQ)_2$, **8**·$(TCNQ)_2$, **9**·$(TCNQ)_4$ and **10**·$(TCNQ)_3$, and **12**·$(TCNQ)_2$ possess different 2D packing motifs of dimers, trimers and tetramers (see above). In all of them the interplanar distances between the oligomers are shorter than 3.3 Å, which can explain conductivities of 10^{-5}–10^{-6} $(\Omega\ cm)^{-1}$, as the energy barrier is lower than in the two previous compounds. In **12**·$(TCNQ)_2$ there are two motifs, one with stacks of equidistant radicals which are known to be good conductors (Molčanov & Kojić-Prodić, 2019; Molčanov *et al.*, 2019*c*). The other is a 2D 'brick wall' and is likely to be a very poor conductor since the interplanar distances between the dimers are >3.35 Å.

The highest conducting compound **9**·$(TCNQ)_4$ reveals a herringbone-like array of pancake-bonded tetramers, where contiguous tetramers are not parallel, but inclined by 16.7° [Table 3, Fig. 4(*e*)]. Therefore, interplanar distances between tetramers cannot be defined; however, close contacts between them are indicated by perpendicular distances of only 2.81 Å. Such short contacts enable electron transfer throughout a herringbone-like layer, resulting in very high conductivity of 10^{-2} $(\Omega\ cm)^{-1}$, which can be compared to neutral radicals such as phenalenyls and dithiazolyls (Lekin *et al.*, 2010; Yu *et al.*, 2011, 2012; Morita *et al.*, 2013), and hybrid salts of $TCNQ^{\delta-}$ with Fe(II) complexes (Üngör *et al.*, 2021*b*).

2.4. Electron paramagnetic resonance study

In the first step, the total spin concentrations were determined from the powder electron paramagnetic resonance (EPR) spectra of the samples at room temperature. The results are shown in Table 6. All powder samples have spin concentrations comparable to N_{mol} except for **8**·$(TCNQ)_2$, whose spin concentration is 1% of N_{mol}. From Table 6 it can be observed that the number of spins regarding the number of molecules differs from sample to sample. **6**·$(TCNQ)_2$ and **12**·$(TCNQ)_2$ have one electron spin per molecule, whereas **9**·$(TCNQ)_4$ has two spins per molecule. These results agree very well with the charge calculations. $\mathbf{1}_2$·Br·$(TCNQ)_2$ and **4**·$(TCNQ)_2$ have about half an electron spin per single molecule. For the rest of the sample one can say the EPR signal is not a property of every molecule, specifically for **8**·$(TCNQ)_2$. Regarding **4**·$(TCNQ)_2$ and **10**·$(TCNQ)_3$, we observed a magnetic transition that is not constant at room temperature and therefore the results show deviation from charge calculations. Further study at higher temperatures is needed to validate the agreement of N_{spin}/N_{mol} with the calculated charges. On the other hand, the recorded single-crystal spectra of **8**·$(TCNQ)_2$ show reasonable intensity, so the low powder spin concentration cannot be assigned to the defects of the structure. The temperature dependence of the EPR spectra studied in the temperature range 100–350 K for the powder samples of $\mathbf{1}_2$·Br·$(TCNQ)_2$, **6**·$(TCNQ)_2$, **9**·$(TCNQ)_4$ and **12**·$(TCNQ)_2$ shows that, by lowering the temperature, the EPR intensity increases (Figs. S19, S20 and S23), and the samples are paramagnetic in the range studied. In these cases of non-cooperative phenomena, electron spins associated with the $TCNQ^{\delta-}$ anions do not interact with each other (non-coupling spins), and the line intensities follow the Curie law which can be calculated using Equation (1),

$$\chi_{EPR} = C/T, \tag{1}$$

where T is the absolute temperature (in K), C is the material-specific Curie constant and χ_{EPR} is the magnetic susceptibility obtained by double integration of the EPR spectra.

4·$(TCNQ)_2$ and **10**·$(TCNQ)_3$ are paramagnetic at room temperature, but they do not follow the Curie law. Instead, EPR intensities show continuous decrease by lowering the temperature, indicating an antiferromagnetic transition.

For a deeper insight into the structure, orientation-dependent measurements of the single crystals at room temperature were performed and the changes of the *g*-value, intensity, linewidth and asymmetry were monitored. The *g*-factor is a second-rank tensor whose anisotropy arises from coupling of the spin angular momentum with the orbital angular momentum. The single crystal is rotated in the EPR cavity around a crystallographic axis and the measured *g*-value is a function of the orientation of the crystal with respect to the field. Presuming a molecular axis, u, v and w are the eigen-directions of the *g*-tensor, the second rank tensor is given by (Wertz & Bolton, 1986)

$$g^2 = g_u^2 \cos^2\varphi + g_v^2 \cos^2\chi + g_w^2 \cos^2\psi, \tag{2}$$

where φ, χ and ψ are the angles between the static magnetic field B and the u, v and w axes, respectively.

The EPR lines of the investigated samples $\mathbf{1}_2$·Br·$(TCNQ)_2$, **4**·$(TCNQ)_2$, **6**·$(TCNQ)_2$, **9**·$(TCNQ)_2$, **10**·$(TCNQ)_3$ and **12**·$(TCNQ)_2$ have a symmetric Lorentzian shape as a result of averaging out both the fine structure and the hyperfine splittings by spin carrier dynamics in the crystal lattices. Nevertheless, for some orientations of the crystals with respect to the static magnetic field, and for highly conducting large samples, an asymmetric line shape known as a Dysonian line was detected (Dyson, 1955). The physical origin of the Dysonian lineshape can be attributed to the fact that the incident microwave field only penetrates a conductive sample to a certain depth, the skin depth (δ), given by the relation

$$\delta = \left(\frac{1}{\sigma\pi f\mu_0}\right)^{1/2}, \tag{3}$$

where σ is the electrical conductivity of the material, μ_0 is the permeability of a vacuum ($4\pi \times 10^{-7}$ H m^{-1}) and f is the microwave frequency.

Despite the averaging effects produced by dynamical spin delocalization and exchange and dipolar coupling, the *g*-factor and EPR linewidth of the **10**·$(TCNQ)_3$ EPR spectra exhibited overly complicated spectra in the single-crystal study so no analysis was carried out. Looking at the complicated spectral shape of **10**·$(TCNQ)_3$ (see Fig. S22), it seems justifiable that there are spectral components regarding a spin crossover, as expected for a triplet excited signal, but they are poorly resolved. It may be interpreted as a triplet with rather small zero-field splitting. Further investigations at high field or lower temperature are necessary.

Angular-dependent peak-to-peak linewidth (Γ) follows the general formula for dipolar broadening (Cheung & Soos, 1978),

$$\Gamma(\theta) = A\left[3\cos^2(\theta-\alpha)-1\right]^2 + B\cos^2(\theta-\alpha) + C, \quad (4)$$

where A, B and C are temperature-dependent, experimentally determined parameters. The angle θ at $\theta = 0^\circ$ marks the position with the largest linewidth, which occurs when the magnetic field is perpendicular to the plane.

Results obtained for **1**$_2$·Br·$(TCNQ)_2$, **4**·$(TCNQ)_2$, **6**·$(TCNQ)_2$, **9**·$(TCNQ)_4$, **10**·$(TCNQ)_3$ and **12**·$(TCNQ)_2$ are shown in Fig. S24–S29 for all three crystal orientations (red, green, blue). Typically, variation of linewidth showing two peaks (one larger and one smaller, separated by approximately 90°) in two rotations about two axes suggest a 2D magnetic ordering and conductivity.

For **1**$_2$·Br·$(TCNQ)_2$, which has a 2D brick wall pattern of pancake-bonded dimers (Fig. S4) parallel to the plane (001), rotations around axes *a* and *b* show two maxima, 90° apart, with considerable variation of linewidth. This is consistent with strong interactions between spins and conductivity in two dimensions, parallel to the plane (001).

4·$(TCNQ)_2$ exhibits the largest linewidth variations (0.05–0.3 mT) among all samples measured. The results support a 2D brick wall arrangement of pancake-bonded tetramers in the plane (001) and the strongest interaction in the direction [110] (*i.e.* direction of stacking). For **6**·$(TCNQ)_2$ a single linewidth peak was observed in each rotation.

Crystals of **8**·$(TCNQ)_2$ were mostly splinters, so it was difficult to establish habitus of the crystals and determine the main crystallographic directions. However, in one of the rotations (Fig. S27) two maxima of linewidth (one smaller, one larger) can be seen. This direction is likely to correspond to the strongest interactions (*i.e.* crystallographic *b* axis).

Since the crystals of **9**·$(TCNQ)_4$ are monoclinic with $\beta \simeq 93^\circ$, three orthogonal directions of rotation can be approximated with crystallographic axes *a*, *b* and *c*. Rotation about the *a* axis showed two maxima of linewidth, whereas the other two rotations had only one maximum.

12·$(TCNQ)_2$ displayed rather narrow lines (<0.1 mT) at all orientations. However, variation of linewidths is in accordance with a 2D spin system: 2D arrangement (brick wall dimers and equidistant stacks) in the plane (001); stacking in two directions, one in the direction of the *a* axis, the other in the [110] direction (*i.e.* along the bisector of the *a* and *b* axes). The repeatable line asymmetries in rotations 1 and 3 of **12**·$(TCNQ)_2$ have been observed which are unique among all samples studied. Taking into account that the conductivity is low, the asymmetry of other samples is more likely to be induced by imperfections. EPR parameters obtained by simulation are presented in Table 6.

In general, as can be seen from Table 7, the extracted *g*-values for the single-crystal measurements are in good agreement with those extracted from the powder samples. A degree of difference in the average *g*-value occurs due to the conductivity and difference in sample size regarding single-crystal and powder samples. The most unreliable parameter for all samples is the asymmetry as it depends on many different factors, see Equation (3). The parameters extracted from Equation (4) are shown in Table S3.

3. Conclusions

We prepared and structurally characterized 14 novel salts of the $TCNQ^{\delta-}$ radical anion with planar organic cations. All of them involve pancake-bonded oligomers (dimers, trimers or tetramers) arranged in extended 2D stacked arrays. Alternating anion and cation layers are held together by C—H···N hydrogen bonds. The most typical array is the brick wall pattern. Owing to the close contacts between the oligomers, the crystals are semiconductors with magnetic interactions and conductivity extending in the plane of stacking.

For a selected seven samples representing each type of stacking pattern (Fig. 4) we have determined the magnetic (EPR) and electric (impedance spectroscopy) properties and correlated them with crystal packing. Single-crystal EPR measurements confirmed that 2D stacked arrays of $TCNQ^{\delta-}$ radicals lead to long-range spin ordering and conductivity in two dimensions, corresponding to the plane of stacking. The most important factor for electrical conductivity is the distance between oligomers within a 2D array, as it facilitates electron transfer from one oligomer to another. Thus the electrical conductivity of **9**·$(TCNQ)_4$ [2.44×10^{-2} $(\Omega\ \mathrm{cm})^{-1}$] is one of the highest among ionic radicals (Morita *et al.*, 2013; Murata *et al.*, 2013). This can be attributed the close contact between the pancake-bonded tetramers which are as short as 2.81 Å.

Though pancake bonding has been considered undesirable for the design of novel conductive materials, it is also energetically favourable and therefore difficult to avoid. However, the present work suggests to reverse the problem: 2D arrays with short distances between radical oligomers are both stable and good conductors. Therefore, this work offers a possible novel strategy for the design of organic conductors.

4. Experimental

4.1. Preparation and IR spectroscopy

All chemicals and solvents used were purchased from commercial sources (Merck, Alfa Aesar, Kemika), were of p.a. or reagent grade and used without additional purification.

Table 7
Summary of the effective *g*-factor global fitting results for single-crystal and powder samples.

Sample	$\{g_1, g_2, g_3\}$ $(g_1 \geq g_2 \geq g_3)$	$g_{average}$	Eigenvectors
$\mathbf{1}_2$·Br·$(TCNQ)_2$	{2.0039, 2.0031, 20.0028}	2.0032	$\begin{pmatrix} -0.1515 & -0.9727 & \pm0.1757 \\ 0.9628 & -0.1855 & \mp0.1966 \\ \pm0.2238 & \pm0.1394 & 0.9646 \end{pmatrix}$
4·$(TCNQ)_2$	{2.0039, 2.0032, 2.0027}	2.0033	$\begin{pmatrix} \pm0.4192 & \mp0.1623 & 0.8933 \\ 0.8003 & -0.1678 & \mp0.4337 \\ 0.2219 & 0.9724 & \pm0.0725 \end{pmatrix}$
6·$(TCNQ)_2$	{2.0040, 2.0035, 2.0026}	2.0034	$\begin{pmatrix} 0.5915 & -0.6356 & \mp0.4962 \\ \pm0.2526 & \mp0.4583 & 0.8626 \\ 0.7657 & 0.6356 & \pm0.0987 \end{pmatrix}$
8·$(TCNQ)_2$	{2.0041, 2.0031, 2.0028}	2.0033	$\begin{pmatrix} \mp0.6780 & \pm0.4404 & 0.5886 \\ 0.7351 & 0.4001 & \pm0.5474 \\ \mp0.0056 & \mp0.8037 & 0.5950 \end{pmatrix}$
9·$(TCNQ)_4$	{2.0039, 2.0032, 2.0028}	2.0033	$\begin{pmatrix} 0.5651 & \pm0.1451 & 0.8122 \\ \mp0.7936 & -0.1736 & \pm0.5832 \\ 0.2256 & \mp0.9741 & 0.0171 \end{pmatrix}$
12·$(TCNQ)_2$	{2.0035, 2.0032, 2.0027}	2.0031	$\begin{pmatrix} 0.6175 & -0.6690 & \pm0.4136 \\ 0.7165 & 0.6954 & \pm0.0551 \\ 0.3245 & -0.2623 & \mp0.9088 \end{pmatrix}$

The compounds were prepared by a modification of our method for the preparation of salts of semiquinone radicals with organic cations (Molčanov *et al.*, 2011, 2012, 2016, 2018*a*, 2019*b*). Powdered TCNQ (20.0 mg) was dissolved in cold acetone (5 ml, at 5°C) until the solution was approximately saturated. Into the solution an excess of solid iodide salt of the appropriate organic cation was added [in the case of $\mathbf{1}_2$·Br·$(TCNQ)_2$ it was bromide]. The beaker was sealed with paraffin and left overnight at room temperature; the next day the acetone solution was decanted and black crystals of the $TCNQ^{\delta-}$ salt were washed with acetone and dried.

Infrared spectra were recorded with KBr pellets using a Bruker Alpha-T spectrometer in the 4000–350 cm^{-1} range.

4.2. X-ray diffraction

Single-crystal measurements were performed on an Oxford Diffraction Xcalibur Nova R (microfocus Cu tube) equipped with an Oxford Instruments CryoJet liquid nitrogen cooling device. The *CrysAlisPRO* package (Rigaku OD, 2018) was used for data reduction and numerical absorption correction.

The structures were solved using *SHELXS97* (Sheldrick, 2015*a*) and refined with *SHELXL-2017* (Sheldrick, 2015*b*). Models were refined using the full-matrix least squares refinement; all non-hydrogen atoms were refined anisotropically. Hydrogen atoms were located in a difference Fourier map and refined either as riding entities or a mixture of free restrained and riding entities.

In the crystals of **2**·$(TCNQ)_2$, **5**·$(TCNQ)_2$, **7**·$(TCNQ)_2$, **13**·$(TCNQ)_2$ and **14**·$(TCNQ)_2$ the cation is disordered about an inversion centre. Thus, two positions of the cation with a p.p. of 0.5 are present, as shown in Fig. S3. To better resolve the structures, the crystals were measured at 100 K; however, in some cases low-temperature data showed no improvement over room temperature. Interestingly, crystals of **13**·$(TCNQ)_2$ at 100 K showed no disorder and the *b* axis doubled compared with the room-temperature structure. It is probable that two phases exist in the same sample, one with ordered and one with disordered cations, since a temperature-driven phase transformation is unlikely here (it would require rotation of an entire *N*-methylpyridinium cation by 180°).

Note that two salts with the iodine-substituted cation **3**·$(TCNQ)_2$ and **6**·$(TCNQ)_2$ crystallize in the rare non-centrosymmetric space group *P*1. The crystal packing of **3**·$(TCNQ)_2$ obviously lacks any symmetry (other than translation), whereas **6**·$(TCNQ)_2$ is pseudocentric with a pseudo-inversion centre coinciding with the centroid of the aromatic ring of the 4-iodo-*N*-methylpyridinium cation. Therefore, the structure can be solved in the space group $P\overline{1}$ with orientational disorder of the cation, similar to those described above. However, refinement of such a structure did not converge, and the disagreement factor *R* remained above 0.20. Refinement in

Table 8
Crystallographic data collection and refinement parameters for variable-temperature X-ray diffraction.

Compound	**1**$_2$·(TCNQ)$_2$·Br	**2**·(TCNQ)$_2$ 100 K	**2**·(TCNQ)$_2$ RT	**3**·(TCNQ)$_2$
Empirical formula	$C_{18}H_{11}Br_{1.50}N_5$	$C_{31}H_{10}N_9$	$C_{31}H_{10}N_9$	$C_{30}H_{15}IN_9$
Formula weight (g mol^{-1})	417.18	508.48	508.48	628.41
Colour	Black	Black	Black	Black
Crystal dimensions (mm)	0.18 × 0.06 × 0.04	0.25 × 0.13 × 0.10	0.25 × 0.13 × 0.10	0.12 × 0.10 × 0.05
Space group	$P\overline{1}$	$P2_1/c$	$P2_1/c$	$P1$
a (Å)	7.2378 (4)	13.2712 (6)	13.3766 (2)	7.1680 (4)
b (Å)	7.7475 (4)	12.5807 (5)	12.8023 (2)	7.6291 (4)
c (Å)	17.8746 (12)	7.7388 (5)	7.78610 (10)	13.6797 (8)
α (°)	83.578 (5)	90	90	78.422 (5)
β (°)	83.241 (5)	90.466 (4)	90.3960 (10)	83.441 (5)
γ (°)	67.104 (5)	90	90	69.680 (5)
Z	2	2	2	1
V (Å^3)	914.53 (10)	1292.04 (11)	1333.35 (3)	686.44 (7)
D_{calc} (g cm^{-3})	1.515	1.266	1.266	1.518
λ (Å)	1.54184 (Cu $K\alpha$)	1.54184 (Cu $K\alpha$)	1.54184 (Cu $K\alpha$)	1.54184 (Cu $K\alpha$)
μ (mm^{-1})	4.415	0.653	0.653	9.464
Θ range (°)	4.99–73.47	4.84–75.70	4.75–75.91	3.30–75.99
T (K)	293 (2)	100 (2)	293 (2)	293 (2)
Diffractometer type	Xcalibur Nova	Xcalibur Nova	Xcalibur Nova	Xcalibur Nova
Range of hkl	$-9 < h < 8$; $-9 < k < 8$; $-19 < l < 22$	$-15 < h < 16$; $-15 < k < 14$; $-9 < l < 9$	$-16 < h < 13$; $-15 < k < 13$; $-9 < l < 9$	$-7 < h < 8$; $-7 < k < 9$; $-15 < l < 17$
Reflections collected	7195	5148	7175	5556
Independent reflections	3677	2569	2655	3390
Observed reflections ($I \geq 2\sigma$)	3245	1751	2368	3380
Absorption correction	Multi-scan	Multi-scan	Multi-scan	Multi-scan
T_{min}, T_{max}	0.2258, 1.0000	0.4314, 1.0000	0.7402, 1.0000	0.5928, 1.0000
R_{int}	0.0267	0.0797	0.0155	0.0367
$R(F)$	0.0659	0.1360	0.0801	0.0421
$R_w(F^2)$	0.2150	0.3914	0.2436	0.1145
Goodness of fit	1.055	1.064	1.063	1.032
H atom treatment	Constrained	Constrained	Constrained	Constrained
No. of parameters	224	190	190	361
No. of restraints	0	58	59	3
$\Delta\rho_{max}$, $\Delta\rho_{min}$, $\Delta\rho_{r.m.s.}$ (eÅ^{-3})	1.054, −0.608, 0.127	1.088, −0.690, 0.132	0.495, −0.466, 0.057	0.536, −1.182, 0.079

Compound	**4**·(TCNQ)$_2$	**5**·(TCNQ)$_2$	**6**·(TCNQ)$_2$	**7**·(TCNQ)$_2$ 100 K
Empirical formula	$C_{37}H_{20}N_9O$	$C_{16}H_8N_5$	$C_{30}H_{15}IN_9$	$C_{15}H_9N_5$
Formula weight (g mol^{-1})	606.62	270.27	628.41	259.27
Colour	Black	Black	Black	Black
Crystal dimensions (mm)	0.40 × 0.15 × 0.12	0.22 × 0.20 × 0.03	0.15 × 0.09 × 0.05	0.38 × 0.32 × 0.05
Space group	$P\overline{1}$	$P\overline{1}$	$P1$	$P\overline{1}$
a (Å)	9.1474 (2)	7.5381 (5)	7.0735 (5)	7.0634 (4)
b (Å)	11.3666 (5)	8.0130 (7)	7.8171 (4)	7.8154 (5)
c (Å)	15.9321 (6)	13.3368 (12)	13.8419 (4)	13.4680 (8)
α (°)	106.234 (4)	103.618 (8)	74.353 (4)	73.628 (5)
β (°)	91.277 (3)	90.811 (6)	88.928 (4)	89.550 (5)
γ (°)	99.804 (3)	115.727 (8)	67.934 (6)	67.258 (6)
Z	2	2	1	2
V (Å^3)	1562.98 (10)	699.07 (11)	680.10 (7)	653.56 (7)
D_{calc} (g cm^{-3})	1.289	1.267	1.534	1.317
λ (Å)	1.54184 (Cu $K\alpha$)	1.54184 (Cu $K\alpha$)	1.54184 (Cu $K\alpha$)	1.54184 (Cu $K\alpha$)
μ (mm^{-1})	0.665	0.648	9.552	0.679
Θ range (°)	4.11–75.96	3.44–76.34	6.28–75.70	3.42–75.92
T (K)	293 (2)	293 (2)	293 (2)	100 (2)
Diffractometer type	Xcalibur Nova	Xcalibur Nova	Xcalibur Nova	Xcalibur Nova
Range of hkl	$-7 < h < 11$; $-13 < k < 14$; $-18 < l < 20$	$-9 < h < 8$; $-9 < k < 9$; $-16 < l < 15$	$-8 < h < 8$; $-9 < k < 9$; $-11 < l < 17$	$-7 < h < 8$; $-6 < k < 9$; $-14 < l < 16$
Reflections collected	13967	4489	5812	4851
Independent reflections	6405	2612	3377	2657
Observed reflections ($I \geq 2\sigma$)	5339	2083	3335	2343
Absorption correction	Multi-scan	Multi-scan	Multi-scan	Multi-scan
T_{min}, T_{max}	0.6377, 1.0000	0.5524, 1.0000	0.4396, 1.0000	0.6578, 1.0000
R_{int}	0.0226	0.0320	0.0317	0.0455
$R(F)$	0.0458	0.0725	0.0625	0.0592
$R_w(F^2)$	0.1796	0.2367	0.1460	0.1813
Goodness of fit	0.712	1.066	1.099	0.996
H atom treatment	Constrained	Constrained	Constrained	Constrained
No. of parameters	424	217	362	190

Table 8 (continued)

Compound	**4**·(TCNQ)$_2$	**5**·(TCNQ)$_2$	**6**·(TCNQ)$_2$	**7**·(TCNQ)$_2$ 100 K
No. of restraints	0	0	5	6
$\Delta\rho_{max}$, $\Delta\rho_{min}$, $\Delta\rho_{r.m.s.}$ (eÅ^{-3})	0.161, −0.146, 0.030	0.359, −0.235, 0.061	2.770, −0.802, 0.143	0.332, −0.313, 0.065

Compound	**7**·(TCNQ)$_2$ RT	**8**·(TCNQ)$_2$	**9**·(TCNQ)$_4$	**10**·(TCNQ)$_3$
Empirical formula	$C_{15}H_9N_5$	$C_{31}H_{16}Br_2N_9$	$C_{31}H_{17}N_9$	$C_{48}H_{26}N_{14}$
Formula weight (g mol^{-1})	259.27	674.35	515.53	798.83
Colour	Black	Black	Black	Black
Crystal dimensions (mm)	0.30 × 0.28 × 0.05	0.41 × 0.28 × 0.04	0.20 × 0.18 × 0.08	0.31 × 0.12 × 0.10
Space group	$P\overline{1}$	$P\overline{1}$	$P2_1/c$	$P\overline{1}$
a (Å)	7.1924(3)	8.0361 (3)	13.0864 (2)	7.8212 (5)
b (Å)	7.8489 (5)	13.0398 (3)	25.3377 (4)	9.7542 (7)
c (Å)	13.6170 (9)	14.2071(4)	7.84030 (10)	13.2653 (7)
α (°)	106.174 (6)	92.624 (2)	90	78.103 (5)
β (°)	90.739 (4)	98.576 (2)	92.6510 (10)	75.829 (5)
γ (°)	112.525 (5)	104.767 (3)	90	82.246 (5)
Z	2	2	4	1
V (Å^3)	675.74 (7)	1418.00 (7)	2596.90 (7)	956.32 (11)
D_{calc} (g cm^{-3})	1.274	1.579	1.319	1.387
λ (Å)	1.54184 (Cu $K\alpha$)	1.54184 (Cu $K\alpha$)	1.54184 (Cu $K\alpha$)	1.54184 (Cu $K\alpha$)
μ (mm^{-1})	0.657	3.943	0.671	0.706
Θ range (°)	6.27–75.85	3.15–75.81	3.77–75.75	3.49–76.47
T (K)	293 (2)	293 (2)	293 (2)	100 (2)
Diffractometer type	Xcalibur Nova	Xcalibur Nova	Xcalibur Nova	Xcalibur Nova
Range of hkl	$-8 < h < 5$; $-9 < k < 9$; $-16 < l < 16$	$-10 < h < 10$; $-16 < k < 15$; $-14 < l < 17$	$-15 < h < 16$; $-25 < k < 31$; $-9 < l < 9$	$-9 < h < 9$; $-12 < k < 12$; $-16 < l < 13$
Reflections collected	5385	12861	13505	8051
Independent reflections	2719	5835	5368	3944
Observed reflections ($I \geq 2\sigma$)	2333	5366	4600	3294
Absorption correction	Multi-scan	Multi-scan	Multi-scan	Multi-scan
T_{min}, T_{max}	0.4767, 1.0000	0.5426, 1.0000	0.6352, 1.0000	0.6772, 1.0000
R_{int}	0.0279	0.0451	0.0180	0.0484
$R(F)$	0.0589	0.0416	0.0468	0.0686
$R_w(F^2)$	0.1930	0.1124	0.1416	0.2069
Goodness of fit	1.018	0.778	0.929	0.928
H atom treatment	Constrained	Constrained	Constrained	Constrained
No. of parameters	190	379	371	280
No. of restraints	6	0	2	0
$\Delta\rho_{max}$, $\Delta\rho_{min}$, $\Delta\rho_{r.m.s.}$ (eÅ^{-3})	0.231, −0.287, 0.044	0.836, −1.020, 0.095	0.257, −0.252, 0.032	0.465, −0.326, 0.083

Compound	**11**$_2$·I·(TCNQ)$_2$	**12**·(TCNQ)$_2$	**13**·(TCNQ)$_2$ 100 K	**13**·(TCNQ)$_2$ RT
Empirical formula	$C_{36}H_{22}Br_2IN_{10}$	$C_{30}H_{14}Br_2N_9$	$C_{30}H_{16}N_9$	$C_{30}H_{16}N_9$
Formula weight (g mol^{-1})	881.35	660.32	502.52	502.52
Colour	Black	Black	Black	Black
Crystal dimensions (mm)	0.31 × 0.14 × 0.12	0.33 × 0.19 × 0.04	0.35 × 0.32 × 0.20	0.20 × 0.17 × 0.07
Space group	$P\overline{1}$	$P\overline{1}$	$P\overline{1}$	$P\overline{1}$
a (Å)	7.5693 (3)	6.6911 (2)	7.7274 (4)	7.2867 (5)
b (Å)	13.0300 (3)	7.8201 (3)	13.1422 (6)	7.7545 (4)
c (Å)	18.5239 (5)	27.6491 (6)	13.3145 (6)	13.1305 (7)
α (°)	105.159 (2)	97.673 (2)	99.902 (4)	92.616 (5)
β (°)	90.971 (3)	90.168 (2)	106.251 (5)	103.414 (5)
γ (°)	98.382 (3)	108.973 (3)	97.225 (4)	113.979 (6)
Z	2	2	2	1
V (Å^3)	1741.67 (9)	1354.24 (8)	1257.00 (11)	651.18 (7)
D_{calc} (g cm^{-3})	1.681	1.619	1.328	1.230
λ (Å)	1.54184 (Cu $K\alpha$)	1.54184 (Cu $K\alpha$)	1.54184 (Cu $K\alpha$)	1.54184 (Cu $K\alpha$)
μ (mm^{-1})	10.252	4.115	0.679	0.640
Θ range (°)	3.55–76.25	3.21–76.29	3.47–75.21	6.31–76.07
T (K)	100 (2)	293 (2)	100 (2)	293 (2)
Diffractometer type	Xcalibur Nova	Xcalibur Nova	Xcalibur Nova	Xcalibur Nova
Range of hkl	$-9 < h < 9$; $-15 < k < 16$; $-23 < l < 21$	$-8 < h < 8$; $-9 < k < 9$; $-23 < l < 34$	$-8 < h < 9$; $-15 < k < 16$; $-16 < l < 15$	$-8 < h < 9$; $-9 < k < 7$; $-16 < l < 14$
Reflections collected	15827	11901	8993	4998
Independent reflections	7163	5582	4926	2624
Observed reflections ($I \geq 2\sigma$)	6810	5100	4067	1975
Absorption correction	Multi-scan	Multi-scan	Multi-scan	Multi-scan
T_{min}, T_{max}	0.3460, 1.0000	0.5628, 1.0000	0.3544, 1.0000	0.7450, 1.0000
R_{int}	0.0504	0.0433	0.0708	0.0210

Table 8 (continued)

Compound	$\mathbf{11}_2$·I·$(TCNQ)_2$	$\mathbf{12}$·$(TCNQ)_2$	$\mathbf{13}$·$(TCNQ)_2$ 100 K	$\mathbf{13}$·$(TCNQ)_2$ RT
$R(F)$	0.0381	0.0434	0.0815	0.1198
$R_w(F^2)$	0.1125	0.1177	0.2380	0.3926
Goodness of fit	0.898	1.042	1.699	1.558
H atom treatment	Constrained	Constrained	Constrained	Constrained
No. of parameters	442	370	352	190
No. of restraints	0	0	0	90
$\Delta\rho_{max}$, $\Delta\rho_{min}$, $\Delta\rho_{r.m.s.}$ (eÅ^{-3})	1.313, −1.421, 0.132	0.873, −0.679, 0.107	0.434, −0.351, 0.085	0.853, −0.783, 0.098

Compound	$\mathbf{14}$·$(TCNQ)_2$ 100 K	$\mathbf{14}$·$(TCNQ)_2$ RT
Empirical formula	$C_{36}H_{16}N_{10}$	$C_{36}H_{16}N_{10}$
Formula weight (g mol^{-1})	588.59	588.59
Colour	Black	Black
Crystal dimensions (mm)	0.21 × 0.09 × 0.08	0.32 × 0.11 × 0.09
Space group	$P\overline{1}$	$P\overline{1}$
a (Å)	7.1249 (13)	7.2179 (10)
b (Å)	7.6572 (13)	7.6887 (14)
c (Å)	14.4249 (10)	14.5445 (13)
α (°)	89.017 (10)	89.176 (10)
β (°)	83.589 (12)	82.570 (9)
γ (°)	68.340 (17)	69.284 (14)
Z	1	1
V (Å^3)	726.6 (2)	748.2 (2)
D_{calc} (g cm^{-3})	1.345	1.306
λ (Å)	1.54184 (Cu $K\alpha$)	1.54184 (Cu $K\alpha$)
μ (mm^{-1})	0.685	0.665
Θ range (°)	6.17–75.55	6.15–74.72
T (K)	100 (2)	293 (2)
Diffractometer type	Xcalibur Nova	Xcalibur Nova
Range of hkl	$-8 < h < 6$; $-9 < k < 9$; $-18 < l < 18$	$-9 < h < 8$; $-9 < k < 9$; $-17 < l < 18$
Reflections collected	5931	6183
Independent reflections	2996	3038
Observed reflections ($I \geq 2\sigma$)	2391	2470
Absorption correction	Multi-scan	Multi-scan
T_{min}, T_{max}	0.6330, 1.0000	0.6757, 1.0000
R_{int}	0.0572	0.0374
$R(F)$	0.1281	0.1078
$R_w(F^2)$	0.3816	0.3477
Goodness of fit	1.481	1.400
H atom treatment	Constrained	Constrained
No. of parameters	217	217
No. of restraints	0	0
$\Delta\rho_{max}$, $\Delta\rho_{min}$, $\Delta\rho_{r.m.s.}$ (eÅ^{-3})	1.251, −0.400, 0.120	0.918, −0.236, 0.080

the space group $P1$ proceeded smoothly; however, a small degree of orientational disorder of the cation is nevertheless present. This could be inferred from the unrealistically elongated N5—C18 bond [which was restrained to 1.40 (1) Å] and unusually small displacement ellipsoid of C18 (Fig. S2). This disorder was too small to be modelled.

Molecular geometry calculations were performed using *PLATON* (Spek, 2003; 2020) and molecular graphics were prepared with *ORTEP-3* (Farrugia, 1997) and *Mercury* (Macrae *et al.*, 2020). Crystallographic and refinement data for the structures reported in this paper are provided in Table 8. CCDC entries 2105173–2105191 contain the supplementary crystallographic data for this paper.

4.3. Electron paramagnetic resonance spectroscopy

EPR spectroscopy was used to determine the magnetic properties of the studied compounds. The single-crystal and powder measurements were carried out on a standard Bruker Elexsys 580 X-band EPR spectrometer, equipped with an Oxford continuous-flow cryostat with a flow of cold N_2 gas, in the range 80–300 K. EPR spectra in the range 300–360 K were recorded on a Varian E-109 X-band spectrometer using a Bruker ER 4111VT variable-temperature unit with a flow of cold N_2 gas. For the powder samples, Suprasil Quartz EPR Sample Tubes were used. The single crystal was evaluated first under a microscope and then by X-ray diffraction. It was aligned with a crystal axis on the EPR holder to ensure the EPR measurements were carried out on single crystals and to avoid twinning or multiple crystals that would affect our EPR measurements. The single crystals were mounted on the quartz rod with a goniometer and EPR spectra were recorded in three mutually perpendicular planes by rotating the crystals around the a, b and c axes at 5° intervals from 0 to 180°. The manganese standard reference Mn^{2+} in MgO was used to calibrate the magnetic field of the EPR spectrometer and consequently the g-value. The radical concentration in each sample was determined by dividing the value of the double

integral of the EPR signal by the mass of the sample. Varian strong pitch was used as a standard to calculate the number of radicals. Spectral simulations were carried out using the *Easyspin* (Stoll & Schweiger, 2006) software working on the *MATLAB* platform (The Mathworks, 2011), and the in-house-made *Mathematica* program was used for the single-crystal spectra (Wolfram Research, 2019).

4.4. Electrical measurements

The electrical conductivities of **1**$_2$·Br·(TCNQ)$_2$, **4**·(TCNQ)$_2$, **6**·(TCNQ)$_2$, **8**·(TCNQ)$_2$, **9**·(TCNQ)$_4$, **10**·(TCNQ)$_3$ and **12**·(TCNQ)$_2$ were measured by impedance spectroscopy (Novocontrol Alpha-AN dielectric analyser) from 0.01 to 1 MHz at temperatures from −80 to 80°C (in steps of 20°C). The measurements were performed on polycrystalline samples pressed into pellets approximately 1 mm-thick. For the electrical contacts, gold electrodes (3.8 mm in diameter) were sputtered on the opposite surfaces of the pellets, except for the **4**·(TCNQ)$_2$ sample, which was measured with Ag electrodes due to difficulties with Au deposition.

Acknowledgements

The authors thank Dr Lidija Androš Dubraja and Dr Sanja Burazer (Rudjer Bošković Institute) for the powder diffraction measurements of the bulk samples and the Rietveld refinement.

Funding information

This work was financed by the Croatian Science Foundation (grant No. IP-2019-04-4674).

References

Abashev, G. G., Vlasova, R. M., Kartenko, N. F., Kuzmin, A. M., Rozhdestvenskaya, I. V., Semkin, V. N., Usov, O. A. & Russkikh, V. S. (1987). *Acta Cryst.* C**43**, 1108–1112.
Akutagawa, T., Saito, G., Kusunoki, M. & Sakaguchi, K. (1996). *Bull. Chem. Soc. Jpn*, **69**, 287–2511.
Akutagawa, T., Takeda, S., Hasegawa, T. & Nakamura, T. (2004). *J. Am. Chem. Soc.* **126**, 291–294.
Alemany, P., Canadell, E., Geng, Y., Hauser, J., Macchi, P., Krämer, K., Decurtins, S. & Liu, S.-X. (2015). *ChemPhysChem*, **16**, 1361–1365.
Ashwell, G. J., Allen, D. W., Kennedy, D. A. & Nowell, I. W. (1982). *Acta Cryst.* B**38**, 2525–2528.
Ashwell, G. J., Allen, J. G., Cross, G. H. & Nowell, I. W. (1983). *Phys. Status Solidi A*, **79**, 455–463.
Ashwell, G. J., Bartlett, V. E., Davies, J. K., Eley, D. D., Wallwork, S. C., Willis, M. R., Harper, A. & Torrance, A. C. (1977*c*). *Acta Cryst.* B**33**, 2602–2607.
Ashwell, G. J., Eley, D. D., Drew, N. J., Wallwork, S. C. & Willis, M. R. (1977*a*). *Acta Cryst.* B**33**, 2598–2602.
Ashwell, G. J., Eley, D. D., Drew, N. J., Wallwork, S. C. & Willis, M. R. (1978). *Acta Cryst.* B**34**, 3608–3612.
Ashwell, G. J., Eley, D. D., Harper, A., Torrance, A. C., Wallwork, S. C. & Willis, M. R. (1977*d*). *Acta Cryst.* B**33**, 2258–2263.
Ashwell, G. J., Eley, D. D., Wallwork, S. C., Willis, M. R., Peachey, G. F. & Wilkos, D. B. (1977*b*). *Acta Cryst.* B**33**, 843–848.
Ashwell, G. J. & Nowell, I. W. (1984). *Phys. Status Solidi A*, **83**, 39–45.
Ashwell, G. J. & Wallwork, S. C. (1979). *Acta Cryst.* B**35**, 1648–1651.
Ashwell, G. J. & Wallwork, S. C. (1985). *Z. Naturforsch. A*, **40**, 726–730.
Ashwell, G. J., Wallwork, S. C., Baker, S. R. & Berthier, P. I. C. (1975*a*). *Acta Cryst.* B**31**, 1174–1178.
Austin, I. G. (1970). *J. Non-Cryst. Solids*, **2**, 474–483.
Ballester, L., Gil, A. M., Gutiérrez, A., Perpiñán, M. F., Azcondo, M. T., Sánchez, A. F., Coronado, E. & Gómez-García, C. J. (2000). *Inorg. Chem.* **39**, 2837–2842.
Ballester, L., Gutiérrez, A., Perpiñán, M. F., Amador, U., Azcondo, M. T., Sánchez, A. F. & Bellitto, C. (1997). *Inorg. Chem.* **36**, 6390–6396.
Beldjoudi, Y., Arauzo, A., Campo, J., Gavey, E. L., Pilkington, M., Nascimento, M. & Rawson, J. M. (2019). *J. Am. Chem. Soc.* **141**, 6875–6889.
Bell, S. E., Field, J. S. & Haines, R. J. (1991). *J. Chem. Soc. Chem. Commun.* pp. 489–491.
Bendikov, M., Wudl, F. & Perepichka, D. F. (2004). *Chem. Rev.* **104**, 4891–4946.
Bigoli, F., Deplano, P., Devillanova, F. A., Girlando, A., Lippolis, V., Mercuri, M. L., Pellinghelli, M. A. & Trogu, E. F. (1996). *Inorg. Chem.* **35**, 5403–5406.
Bodegom, B. van, de Boer, J. L. & Vos, A. (1977). *Acta Cryst.* B**33**, 602–604.
Bosch, A. & van Bodegom, B. (1977). *Acta Cryst.* B**33**, 3013–3021.
Brook, D. J. R. & Koch, T. H. (1997). *J. Mater. Chem.* **7**, 2381–2385.
Bryce, M. R., Moore, A. J., Bates, P. A., Hursthouse, M. B., Liu, Z.-X. & Nowak, M. J. (1988). *J. Chem. Soc. Chem. Commun.* pp. 1441.
Bryce, M. R., Moore, A. J., Hasan, M., Ashwell, G. J., Fraser, A. T., Clegg, W., Hursthouse, M. B. & Karaulov, A. I. (1990). *Angew. Chem. Int. Ed. Engl.* **29**, 1450–1452.
Caballero, A., Zapata, F., White, N. G., Costa, P. J., Félix, V. & Beer, P. D. (2012). *Angew. Chem. Int. Ed.* **51**, 1876–1880.
Chen, X., Gao, F. & Yang, W. (2016). *Sci. Rep.* **6**, 29314.
Chen, Y. C., Liu, G. X., Wang, P. F., Xu, H., Ren, X. M., Song, Y. & Sui, Y. X. (2007). *Polyhedron*, **26**, 1781–1786.
Chen, Y.-C., Wang, P.-F., Liu, G.-X., Xu, H., Ren, X.-M., Song, Y. & Ni, Z.-P. (2008). *J. Phys. Chem. Solids*, **69**, 2445–2452.
Cheung, T. T. P. & Soos, Z. G. (1978). *J. Chem. Phys.* **69**, 3845–3853.
Cui, Z.-H., Lischka, H., Beneberu, H. Z. & Kertesz, M. (2014*a*). *J. Am. Chem. Soc.* **136**, 5539–5542.
Cui, Z.-H., Lischka, H., Beneberu, H. Z. & Kertesz, M. (2014*b*). *J. Am. Chem. Soc.* **136**, 12958–12965.
Cui, Z.-H., Lischka, H., Mueller, T., Plasser, F. & Kertesz, M. (2014*c*). *ChemPhysChem*, **15**, 165–176.
Diezt, K., Endres, H., Keller, H. J. & Moroni, W. (1981). *Z. Naturforsch. B*, **36b**, 952–955.
Dyson, F. H. (1955). *Phys. Rev.* **98**, 349–359.
Endres, H. (1982). *Angew. Chem. Int. Ed. Engl.* **21**, 524–524.
Endres, H., Keller, H. J., Moroni, W., Nöthe, D. & Dong, V. (1978*a*). *Acta Cryst.* B**34**, 1703–1705.
Endres, H., Keller, H. J., Moroni, W., Nöthe, D. & Dong, V. (1978*b*). *Acta Cryst.* B**34**, 1823–1827.
Farrugia, L. J. (1997). *J. Appl. Cryst.* **30**, 565–565.
Filhol, A. & Thomas, M. (1984). *Acta Cryst.* B**40**, 44–59.
Filhol, A., Zeyen, C. M. E., Chenavas, P., Gaultier, J. & Delhaes, P. (1980). *Acta Cryst.* B**36**, 2719–2726.
Fotović, L. & Stilinović, V. (2020). *CrystEngComm*, **22**, 4039–4046.
Ganesan, V., Rosokha, S. V. & Kochi, J. K. (2003). *J. Am. Chem. Soc.* **125**, 2559–2571.
Grebe, J., Geiseler, G., Harms, K., Neumüller, B. & Dehnicke, K. (1999). *Angew. Chem. Int. Ed.* **38**, 222–225.
Groom, C. R., Bruno, I. J., Lightfoot, M. P. & Ward, S. C. (2016). *Acta Cryst.* B**72**, 171–179.
Grossel, M. C. & Weston, S. C. (1992). *J. Chem. Soc. Chem. Commun.* pp. 1510–1512.
Harms, R., Keller, H. J., Nöthe, D. & Wehe, D. (1982). *Acta Cryst.* B**38**, 2838–2841.
Herbstein, F. H. & Kapon, M. (2008). *Crystallogr. Rev.* **14**, 3–74.

Hicks, R. G. (2011). *Nat. Chem.* **3**, 189–191.
Hoekstra, A., Spoelder, T. & Vos, A. (1972). *Acta Cryst.* B**28**, 14–25.
Huang, J. & Kertesz, M. (2007). *J. Am. Chem. Soc.* **129**, 1634–1643.
Huang, J., Kingsbury, S. & Kertesz, M. (2008). *Phys. Chem. Chem. Phys.* **10**, 2625–2635.
Hünig, S. (1990). *Pure Appl. Chem.* **62**, 395–406.
Itkis, M. E., Chi, X., Cordes, A. W. & Haddon, R. C. (2002). *Science*, **296**, 1443–1445.
Jakupec, N., Fotović, L. & Stilinović, V. (2020). *CrystEngComm*, **22**, 8142–8150.
Keller, H. J., Steiger, W. & Werner, M. (1981). *Z. Naturforsch. B*, **36**, 1187–1189.
Kertesz, M. (2019). *Chem. Eur. J.* **25**, 400–416.
Kistenmacher, T. J., Emge, T. J., Bloch, A. N. & Cowan, D. O. (1982). *Acta Cryst.* B**38**, 1193–1199.
Kistenmacher, T. J., Phillips, T. E. & Cowan, D. O. (1974). *Acta Cryst.* B**30**, 763–768.
Kojić-Prodić, B. & Molčanov, K. (2008). *Acta Chim. Slov.* **55**, 692–708.
Konno, M. & Saito, Y. (1981). *Acta Cryst.* B**37**, 2034–2043.
Kubota, H., Takahashi, Y., Harada, J. & Inabe, T. (2014). *Cryst. Growth Des.* **14**, 5575–5584.
Lau, C.-P., Singh, P., Cline, S. J., Seiders, R., Brookhart, M., Marsh, W. E., Hodgson, D. J. & Hatfield, W. E. (1982). *Inorg. Chem.* **21**, 208–212.
Lekin, K., Winter, S. M., Downie, L. E., Bao, X., Tse, J. S., Desgreniers, S., Secco, R. A., Dube, P. A. & Oakley, R. T. (2010). *J. Am. Chem. Soc.* **132**, 16212–16224.
Liu, G.-X., Guo, X., Yang, H., Nishihara, S. & Ren, X.-M. (2011). *J. Chem. Crystallogr.* **41**, 1262–1267.
Liu, G.-X., Xu, H., Ren, X.-M. & Sun, W.-Y. (2008). *CrystEngComm*, **10**, 1574–1582.
Logothetis, T. A., Meyer, F., Metrangolo, P., Pilati, T. & Resnati, G. (2004). *New J. Chem.* **28**, 760–763.
Lu, J., Nafady, A., Abrahams, B. F., Abdulhamid, M., Winther-Jensen, B., Bond, A. M. & Martin, L. L. (2017). *Aust. J. Chem.* **70**, 997–1005.
Lu, J., Qu, X., Peleckis, G., Boas, J. F., Bond, A. M. & Martin, L. L. (2011). *J. Org. Chem.* **76**, 10078–10082.
Lunelli, B. & Pecile, C. (1970). *J. Chem. Phys.* **52**, 2375–2384.
Macrae, C. F., Sovago, I., Cottrell, S. J., Galek, P. T. A., McCabe, P., Pidcock, E., Platings, M., Shields, G. P., Stevens, J. S., Towler, M. & Wood, P. A. (2020). *J. Appl. Cryst.* **53**, 226–235.
Magonov, S. N., Kempf, S., Rotter, H. & Cantow, H.-J. (1991). *Synth. Met.* **40**, 73–86.
Malatesta, V., Millini, R. & Montanari, L. (1995). *J. Am. Chem. Soc.* **117**, 6258–6264.
Martin, L. L., Lu, J., Nafady, A., Le, T. H., Siriwardana, A. I., Qu, X., Traore, D. A. Q., Wilce, M. & Bond, A. M. (2012). *Aust. J. Chem.* **65**, 935–941.
The MathWorks (2011). *MATLAB*. The MathWorks Inc., Natick, Massachusetts, USA.
Melen, R. L., Less, R. J., Pask, C. M. & Rawson, J. M. (2016). *Inorg. Chem.* **55**, 11747–11759.
Mercuri, M. L., Deplano, P., Pilia, L., Serpe, A. & Artizzu, F. (2010). *Coord. Chem. Rev.* **254**, 1419–1433.
Miller, J. S., Zhang, J. H., Reiff, W. M., Dixon, D. A., Preston, L. D., Reis, A. H., Gebert, E., Extine, M., Troup, J. *et al.* (1987). *J. Phys. Chem.* **91**, 4344–4360.
Mínguez Espallargas, G., Zordan, F., Arroyo Marín, L., Adams, H., Shankland, K., van de Streek, J. & Brammer, L. (2009). *Chem. Eur. J.* **15**, 7554–7568.
Mochida, T., Takazawa, K., Takahashi, M., Takeda, M., Nishio, Y., Sato, M., Kajita, K., Mori, H., Matsushita, M. M. & Sugawara, T. (2008). *J. Phys. Soc. Jpn*, **74**, 2214–2216.
Molčanov, K., Jelsch, C., Landeros-Rivera, B., Hernández-Trujillo, J., Wenger, E., Stilinović, V., Kojić-Prodić, B. & Escudero-Adán, E. C. (2019*a*). *Cryst. Growth Des.* **19**, 391–402.
Molčanov, K. & Kojić-Prodić, B. (2019). *IUCrJ*, **6**, 156–166.
Molčanov, K., Kojić-Prodić, B., Babić, D., Pajić, D., Novosel, N. & Zadro, K. (2012). *CrystEngComm*, **14**, 7958–7964.
Molčanov, K., Kojić-Prodić, B., Babić, D., Žilić, D. & Rakvin, B. (2011). *CrystEngComm*, **13**, 5170–5178.
Molčanov, K., Milašinović, V., Ivić, N., Kolarić, D. & Kojić-Prodić, B. (2019*b*). *CrystEngComm*, **21**, 6920–6928.
Molčanov, K., Milašinović, V. & Kojić-Prodić, B. (2019*c*). *Cryst. Growth Des.* **19**, 5967–5980.
Molčanov, K., Mou, Z., Kertesz, M., Kojić-Prodić, B., Stalke, D., Demeshko, S., Šantić, A. & Stilinović, V. (2018*b*). *Chem. Eur. J.* **24**, 8292–8297.
Molčanov, K., Stalke, D., Šantić, A., Demeshko, S., Stilinović, V., Mou, Z., Kertesz, M. & Kojić-Prodić, B. (2018*a*). *CrystEngComm*, **20**, 1862–1873.
Molčanov, K., Stilinović, V., Šantić, A., Maltar-Strmečki, N., Pajić, D. & Kojić-Prodić, B. (2016). *Cryst. Growth Des.* **16**, 4777–4782.
Moore, A. J., Batsanov, A. S., Bryce, M. R., Howard, J. A. K., Khodorkovsky, V., Shapiro, L. & Shames, A. (2001). *Eur. J. Org. Chem.* **2001**, 73–78.
Morimoto, T., Nagai, M., Minowa, Y., Ashida, M., Yokotani, Y., Okuyama, Y. & Kani, Y. (2019). *Nat. Commun.* **10**, 2662, 1–8.
Morita, Y., Murata, T. & Nakasuji, K. (2013). *Bull. Chem. Soc. Jpn*, **86**, 183–197.
Mou, Z. & Kertesz, M. (2017). *Angew. Chem. Int. Ed.* **56**, 10188–10191.
Mukai, K., Jinno, S., Shimobe, Y., Azuma, N., Hosokoshi, Y., Inoue, K., Taniguchi, M., Misaki, Y. & Tanaka, K. (2001). *Polyhedron*, **20**, 1537–1544.
Murata, T., Morita, Y., Fukui, K., Tamaki, K., Yamochi, H., Saito, G. & Nakasuji, K. (2006). *Bull. Chem. Soc. Jpn*, **79**, 894–913.
Murata, T., Nishimura, K. & Saito, G. (2007). *Mol. Cryst. Liq. Cryst.* **466**, 101–112.
Murata, T., Yamamoto, Y., Yakiyama, Y., Nakasuji, K. & Morita, Y. (2013). *Bull. Chem. Soc. Jpn*, **86**, 927–939.
Nakano, T. (2014). (Ed). *π-Stacked Polymers and Molecules*, Tokyo: Springer.
Nikolayenko, V. I., Barbour, L. J., Arauzo, A., Campo, J., Rawson, J. M. & Haynes, D. A. (2017). *Chem. Commun.* **53**, 11310–11313.
Nishijo, J., Miyazaki, A. & Enoki, T. (2004). *Bull. Chem. Soc. Jpn*, **77**, 715–727.
Nishimura, K., Hirate, S. & Saito, G. (2002). *Mol. Cryst. Liq. Cryst.* **376**, 213–218.
Novoa, J. J., Stephens, P. W., Weerasekare, M., Shum, W. W. & Miller, J. S. (2009). *J. Am. Chem. Soc.* **131**, 9070–9075.
O'Hare, D., Ward, M. D. & Miller, J. S. (1990). *Chem. Mater.* **2**, 758–763.
Ormond-Prout, J. E., Smart, P. & Brammer, L. (2012). *Cryst. Growth Des.* **12**, 205–216.
Park, J. S., Park, J., Yang, Y. J., Tran, T. T., Kim, I. S. & Sessler, J. L. (2018). *J. Am. Chem. Soc.* **140**, 7598–7604.
Phan, H., Benjamin, S. M., Steven, E., Brooks, J. S. & Shatruk, M. (2015). *Angew. Chem. Int. Ed.* **54**, 823–827.
Podzorov, V. (2010). *Nat. Mater.* **9**, 616–617.
Preuss, K. E. (2014). *Polyhedron*, **79**, 1–15.
Qu, X., Lu, J., Zhao, C., Boas, J. F., Moubaraki, B., Murray, K. S., Siriwardana, A., Bond, A. M. & Martin, L. L. (2011). *Angew. Chem. Int. Ed.* **50**, 1589–1592.
Radváková, A., Kazheva, O. N., Chekhlov, A. N., Dyachenko, O. A., Kucmin, M., Kajňaková, M., Feher, A. & Starodub, V. A. (2010). *J. Phys. Chem. Solids*, **71**, 752–757.
Ratera, I. & Veciana, J. (2011). *Chem. Soc. Rev.* **40**, 303–349.
Renka, S., Klaser, T., Burazer, S., Mošner, P., Kalenda, P., Šantić, A. & Moguš-Milanković, A. (2020). *Nanomaterials*, **10**, 2515:1–13.
Rigaku OD (2018). *CrysAlis PRO*. Rigaku Oxford Diffraction, Yarnton, Oxfordshire, England.
Rindorf, G., Thorup, N. & Kamaras, K. (1988). *Synth. Met.* **25**, 189–195.

Rosokha, S. V. & Kochi, J. K. (2007). *J. Am. Chem. Soc.* **129**, 3683–3697.
Rosokha, S. V., Lu, J., Rosokha, T. Y. & Kochi, J. K. (2009). *Phys. Chem. Chem. Phys.* **11**, 324–332.
Sandman, D., Epstein, A. J., Holmes, T. J., Lee, J.-S. & Titus, D. D. (1980). *J. Chem. Soc. Perkin Trans. 2*, pp. 1578–1585.
Sanvito, S. (2011*a*). *Chem. Soc. Rev.* **40**, 3336–3355.
Sanvito, S. (2011*b*). *Nat. Mater.* **10**, 484–485.
Schultz, A. J., Stucky, G. D., Blessing, R. H. & Coppens, P. (1976). *J. Am. Chem. Soc.* **98**, 3194–3201.
Sheldrick, G. M. (2015*a*). *Acta Cryst.* A**71**, 3–8.
Sheldrick, G. M. (2015*b*). *Acta Cryst.* C**71**, 3–8.
Shirotani, I. & Kobayashi, H. (1973). *Bull. Chem. Soc. Jpn*, **46**, 2595–2596.
Spek, A. L. (2003). *J. Appl. Cryst.* **36**, 7–13.
Spek, A. L. (2020). *Acta Cryst.* E**76**, 1–11.
Stein, D., Sitzmann, H. & Boese, R. (1991). *J. Organomet. Chem.* **421**, 275–283.
Steiner, T. (2002). *Angew. Chem. Int. Ed.* **41**, 48–76.
Stoll, S. & Schweiger, A. (2006). *J. Magn. Reson.* **178**, 42–55.
Sutton, A. L., Abrahams, B. L., D'Alessandro, D. M., Hudson, T. A., Robson, R. & Usov, P. M. (2016). *CrystEngComm*, **18**, 8906–8914.
Takagi, S., Nakao, K. & Nakatsu, K. (1994). *J. Phys. Soc. Jpn*, **63**, 271–282.
Tian, Y.-H. & Kertesz, M. (2011). *J. Phys. Chem. A*, **115**, 13942–13949.
Üngör, Ö., Burrows, M., Liu, T., Bodensteiner, M., Adhikari, Y., Hua, Z., Casas, B., Balicas, L., Xiong, P. & Shatruk, M. (2021*a*). *Inorg. Chem.* **60**, 10502–10512.
Üngör, Ö., Choi, E. S. & Shatruk, M. (2021*b*). *Chem. Sci.* **12**, 10765–10779.
Usov, O. A., Burshtein, I. A., Kartenko, N. F., Rozhdestvenskaya, I. V., Vlasova, R. M., Semkin, V. N., Abashev, G. G. & Russkikh, V. S. (1991). *Acta Cryst.* C**47**, 1851–1854.
Veciana, J., Arćon, D., Deumal, M., Inoue, K., Kinoshita, M., Novoa, J. J., Palacio, F., Prassides, K., Rawson, J. M. & Rovira C. (2011). (Eds) *π-Electron magnetism: From molecules to magnetic materials*, Vol. 100. Berlin, Heidelberg: Springer.
Visser, R. J. J., Bouwmeester, H. J. M., de Boer, J. L. & Vos, A. (1990*a*). *Acta Cryst.* C**46**, 852–856.
Visser, R. J. J., Bouwmeester, H. J. M., de Boer, J. L. & Vos, A. (1990*c*). *Acta Cryst.* C**46**, 860–864.
Visser, R. J. J., de Boer, J. L. & Vos, A. (1990*b*). *Acta Cryst.* C**46**, 857–860.
Visser, R. J. J., de Boer, J. L. & Vos, A. (1990*d*). *Acta Cryst.* C**46**, 869–871.
Visser, R. J. J., de Boer, J. L. & Vos, A. (1990*f*). *Acta Cryst.* C**46**, 864–866.
Visser, R. J. J., van Smaalen, S., de Boer, J. L. & Vos, A. (1990*e*). *Acta Cryst.* C**46**, 867–869.
Waclawek, W., Wallwork, S. C., Ashwell, G. J. & Chaplain, E. J. (1983). *Acta Cryst.* C**39**, 131–134.
Wertz, J. E. & Bolton, J. R. (1986). *Electron Paramagnetic Resonance*. New York: Chapman and Hall.
Wolfram Research (2019). *Mathematica*. Version 11.2. Wolfram Research Inc., Champaign, IL, USA.
Yu, X., Mailman, A., Dube, P. A., Assoud, A. & Oakley, R. T. (2011). *Chem. Commun.* **47**, 4655–4657.
Yu, X., Mailman, A., Lekin, K., Assoud, A., Robertson, C. M., Noll, B. C., Campana, C. F., Howard, J. A. K., Dube, P. A. & Oakley, R. T. (2012). *J. Am. Chem. Soc.* **134**, 2264–2275.